

PERFORMANCE OPTIMISATION AND EFFICIENT USER GROUPING OF MU-MIMO  
FOR INDOOR OPTICAL WIRELESS COMMUNICATION SYSTEMS



PERFORMANCE OPTIMISATION AND EFFICIENT USER GROUPING OF MU-MIMO  
FOR INDOOR OPTICAL WIRELESS COMMUNICATION SYSTEMS

A Dissertation Presented to  
The Graduate School of Bangkok University

In Partial Fulfillment  
of the Requirements for the Degree  
Doctor of Engineering in Electrical and Computer Engineering

by

Jariya Panta

2021

Copyright of Bangkok University

This Dissertation has been approved by  
the Graduate School  
Bangkok University

Title: Performance Optimisation and Efficient User Grouping of MU-MIMO  
for Indoor Optical Wireless Communication Systems

Author: Jariya Panta

Thesis Committee:

Thesis Advisor



\_\_\_\_\_  
(Assoc. Prof. Dr. Poompat Saengudomlert)

Thesis Co-Advisor



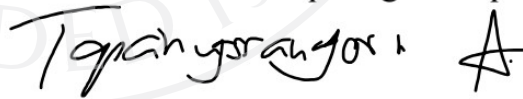
\_\_\_\_\_  
(Dr. Karel L. Sterckx)

Graduate Program Director



\_\_\_\_\_  
(Assoc. Prof. Dr. Chakkaphong Suthaputchakun)

External Representative



\_\_\_\_\_  
(Assoc. Prof. Dr. Attaphongse Taparugssanagorn)



\_\_\_\_\_  
(Asst. Prof. Dr. Wisan Patchoo)

Dean of the School of Engineering

15 / 8 / 2022

Panta, J. Doctor of Engineering in Electrical and Computer Engineering,

August 2022. Graduate School, Bangkok University

Performance Optimisation and Efficient User Grouping of MU-MIMO for Indoor Optical Wireless Communication Systems (93 pp.)

Advisor of Dissertation: Poompat Saengudomlert, Ph.D.

### ABSTRACT

Multiple-input multiple-output (MIMO) in combination with orthogonal frequency division multiplexing (OFDM) is an attractive technique to provide the spectral efficiency and high data transmission rates in optical wireless communications (OWC) systems using light emitting diode (LED) light sources, where the modulation bandwidth of LED is limited. To investigate the performance of the system, indoor MIMO-OFDM OWC systems supporting a single user terminal is considered. However, the performance is limited because of strong correlation among propagation paths dominated by line-of-sight (LOS) components. To mitigate such effects, the receiver front-end design of MIMO-OFDM is investigated to reduce MIMO channel correlation in OWC. In addition, to utilize the OWC broadcast nature, multiuser MIMO-OWC systems have been investigated. When there are multiple user terminals in the same room, there is a challenge to eliminate the multi-user interference (MUI), which affects the transmission performance at each user's receiver. In order to suppress the MUI, block diagonalization (BD) precoding is applied. However, BD prevents only interference among individual users. To further prevent interference among individual data streams of each user, singular value

decomposition (SVD) is applied. Nevertheless, BD precoding is not applicable when the number of photo diodes (PDs) exceeds the number of LED transmitters.

Therefore, to further improve the system performance measured in terms of the bit error rate (BER), this research considers LED transmitter distribution in addition to angular diversity based on tilting receiver PDs. In the first half of the thesis, the research studies the performance of indoor SVD-based MIMO-OFDM OWC systems. In addition, since SVD decomposes the MIMO channel into parallel sub-channels with different path losses, the bit loading technique is utilized. In the second half of the thesis, the research considers a lot of user devices in the same room, yielding more PDs than LEDs. To overcome the limitation of BD precoding, user grouping is performed, and time division multiplexing (TDM) is applied with BD precoding for each user group.

In particular, this research focus on optimising the BER performance of SVD-based MIMO-OFDM OWC systems under the impact of the OFDM symbol design, the configuration of MIMO transmitters, the required data rates, the available bandwidth, and the angular diversity based on tilting receiver PDs. The results show that the  $9 \times 4$ -MIMO system is the optimal configuration in term of the large coverage of low BER regions and low computation complexity for the  $5\text{m} \times 5\text{m}$  room. In addition, polar angle tilting of PDs can effectively improve the BER performance. In the case of light dimming control with a low total transmit optical power, the system can benefit from a high multiplexing gain with a large tilting polar angle, as indicated by improved condition numbers of MIMO channel matrices.

For multiuser systems, user grouping methods are proposed based on pairwise interference considerations among users in the same group. The proposed method can

be implemented through integer linear programming (ILP), which requires less computation than exhaustive search. Numerical results on the average minimum user throughputs over random scenarios indicate that the proposed hybrid method can significantly outperform random user grouping, and performs reasonably well compared to exhaustive search. Finally, it is demonstrated that, when BD precoding greatly attenuates desired user signals, user grouping can help improve the minimum user throughputs even through BD precoding can support all users as a single group.

*Keywords: Multiple-input multiple-output, Orthogonal frequency division multiplexing, Optical wireless communications, Multi-user, Block diagonalization, Singular value decomposition, User grouping, Optimisation, Time division multiplexing.*

Approved: \_\_\_\_\_

Signature of Advisor

## ACKNOWLEDGMENT

First and foremost, I would like to express my sincere gratitude to my advisor, Assoc. Prof. Dr. Poompat Saengudomlert from the bottom of my heart for his excellent guidance, patience, motivation and constant encouragement which really help me to complete my Ph.D study. I could not have imagined having a better advisor and mentor for my Ph.D. life.

I would like to express my gratitude to my co-advisor, Dr. Karel L. Sterckx for providing valuable suggestions that helped guide this entire research.

Besides my advisor, I would like to give my sincere thanks convey to my special co-advisor, Prof.Dr. Anh T. Pham for his kind considerable and valuable comments and suggestions during my study at The University of Aizu, Japan. It has been an amazing experience working with all students in Computer Communications lab (CCL), thanks to everyone from Aizu I have worked with and from whom I have learned so much. Thank you for all the great memories that I will never forget.

Additionally, everything would not have been possible without the mainly support from the scholarship donor, the Royal Golden Jubilee (RGJ) Ph.D. program by the Thailand Research Fund (TRF), who financed my research.

My sincere thanks also goes to my professors and my examination committee members Dr. Attaphongse Taparugssanagorn, Asst. Prof. Dr. Chakkaphong uthaputchakun, Dr. Wareed S. Mohammed and Dr. Romuald Jolivot for their comments and suggestions to my thesis study.

In addition, I would like to offer my special thanks to all the academics who helped me get to this stage.

Last but not the least, I would like to take this opportunity to express my deepest gratitude and thank to my family, especially my parents, spouse, and my adopted daughter for their love, moral support and encouragement. They are my guiding light and lucky stars in my life. In addition, I would like to thank you all of my friends and my colleagues for all the entertainment and emotional support.

My heartfelt thanks.





## TABLE OF CONTENTS

	Page
ABSTRACT.....	iii
ACKNOWLEDGMENT.....	vi
LIST OF TABLES.....	xi
LIST OF FIGURES.....	xii
CHAPTER 1: INTRODUCTION.....	1
1.1 Rationale and Problem Statement.....	1
1.2 Research Questions.....	6
1.3 Research Aims.....	7
1.4 Scopes and Limitations.....	8
1.5 Research Outlines.....	8
CHAPTER 2: LITERATURE REVIEW.....	9
2.1 Overview of OWC.....	9
2.2 Overview of OFDM.....	11
2.3 Overview of OFDM for OWC.....	14
2.3.1 Fundamentals of Flip-OFDM Transmission System.....	17
2.4 Overview of MIMO.....	19
2.4.1 Parallel Decomposition of the MIMO Channel.....	20
2.5 MIMO OFDM using SVD.....	22
2.6 MU-MIMO in OWC.....	24
CHAPTER 3: METHODOLOGY.....	28
3.1 Single User MIMO for an Indoor OWC System.....	28

## TABLE OF CONTENTS (Continued)

	Page
CHAPTER 3: METHODOLOGY (Continued)	
3.1.1 System Model Configurations of Single-User MIMO.....	28
3.1.2 Transmission System of MIMO Flip-OFDM Using SVD.....	31
3.1.3 Bit Loading Technique.....	40
3.1.4 Transmit Optical Power Analysis for MIMO Flip-OFDM.....	41
3.1.5 BER Performance Analysis with bit loading.....	44
3.2 MU-MIMO for an Indoor OWC System.....	46
3.2.1 System Configurations of MU-MIMO.....	46
3.2.2 Transmitted and Received Signals.....	47
3.2.3 BD Precoding and Combining.....	50
3.2.4 User Throughputs.....	52
3.2.5 Heuristics for User Grouping.....	53
3.2.6 ILP Formulation for User Grouping.....	55
CHAPTER 4: SIMULATION RESULTS AND DISCUSSION.....	58
4.1 Single-User MIMO for an Indoor OWC System.....	58
4.1.1 Simulation Parameters and Setups.....	58
4.1.2 Optimisation of OFDM Symbol.....	59
4.1.3 MIMO Transmitter Configurations.....	61
4.1.4 Polar Angle Tilting of PDs and Dimming Control.....	65
4.1.5 Computational Complexity.....	70
4.2 Multiuser MIMO for an Indoor OWC System.....	72

## TABLE OF CONTENTS (Continued)

	Page
CHAPTER 4: SIMULATION RESULTS AND DISCUSSION	
(Continued)	
4.2.1 Simulation Parameters and Setups.....	72
4.2.2 Example User Grouping Scenarios.....	73
4.2.3 Average Minimum User Throughputs.....	77
4.2.4 Comparison of Computational Complexity.....	81
4.2.5 User Grouping for Throughput Improvements when $M_r \leq M_t$ .....	82
CHAPTER 5: CONCLUSION AND RECOMMENDATIONS .....	85
BIBLIOGRAPHY.....	87
BIODATA.....	93

## LIST OF TABLES

	Page
Table 4.1	Simulation parameters for the SVD-based MIMO-OFDM OWC systems.....59
Table 4.2	The condition numbers of 4×4-, 9×4-, and 16×4-MIMO channel matrices for various tilting polar angles of PDs.....71
Table 4.3	Simulation parameters for MU-MIMO OWC systems.....72
Table 4.4	User and PD locations for scenario 1.....75
Table 4.5	User and PD locations for scenario 2.....76
Table 4.6	Minimum user throughputs for scenario 1.....76
Table 4.7	Minimum user throughputs for scenario 2.....77
Table 4.8	Percentages of random scenarios in which each method is chosen by the hybrid method.....81
Table 4.9	Average run times for the hybrid method and the exhaustive method.....82

## LIST OF FIGURES

	Page
Figure 2.1	LOS propagation model.....11
Figure 2.2	(a) single-carrier transmission and (b) multicarrier transmission.....12
Figure 2.3	Spectra of (a) FDM carriers and (b) OFDM subcarriers.....13
Figure 2.4	OFDM transmission system diagram.....15
Figure 2.5	Flip-OFDM transmission system diagram.....18
Figure 2.6	MIMO transmission system.....19
Figure 2.7	MIMO transmission system using SVD.....21
Figure 2.8	The structure of MIMO OFDM transmitter using SVD.....23
Figure 2.9	The structure of MIMO OFDM receiver using SVD.....24
Figure 2.10	The structure of a MU-MIMO broadcasting system.....25
Figure 3.1	Configuration of the single user indoor MIMO OWC system and its spherical coordinates.....29
Figure 3.2	(a) The configuration of the proposed transceiver orientation model, (b) The coordinate of the proposed transceiver orientation model.....29
Figure 3.3	(a) Top view of the 4×4-MIMO, (b) Top view of the 9×4-MIMO, (c) Top view of the 16×4-MIMO.....31
Figure 3.4	Top view of the considered receiver positions.....31
Figure 3.5	The transmission side of the MIMO-flip-OFDM transmission system using SVD.....33
Figure 3.6	The receiving side of the MIMO-flip-OFDM transmission system using SVD.....34

## LIST OF FIGURES (Continued)

	Page
Figure 3.7 Room dimension and coordinates (in m) of the indoor MU-MIMO OWC system.....	47
Figure 3.8 Schematic diagram of indoor MU-MIMO OWC .....	48
Figure 4.1 BER versus utilized BW (MHz) of 4×4-, 9×4- and 16×4-MIMO systems at R1: (2.5,2.5).....	60
Figure 4.2 BER versus utilized BW (MHz) of 4×4-, 9×4- and 16×4-MIMO systems at R2: (1,1).....	60
Figure 4.3 BER versus $P_T^{\text{total}}$ of 4 × 4-, 9 × 4- and 16 × 4-MIMO systems at R1: (2.5,2.5) and R2: (1,1).....	62
Figure 4.4 3D plot of BER of 4 × 4-MIMO with $P_T^{\text{total}} = 45$ dBm.....	63
Figure 4.5 3D plot of BER of 9× 4-MIMO with $P_T^{\text{total}} = 45$ dBm.....	63
Figure 4.6 3D plot of BER of 16× 4-MIMO with $P_T^{\text{total}} = 45$ dBm.....	64
Figure 4.7 CDF of BER of 4×4-, 9×4-, and 16×4-MIMO systems with $P_T^{\text{total}} = 45$ dBm.....	65
Figure 4.8 BER versus polar angle of 4×4- and 9×4-MIMO systems with $P_T^{\text{total}} = 40$ dBm.....	66
Figure 4.9 BER versus $P_T^{\text{total}}$ for tilting polar angles of PDs for 4×4- and 9×4-MIMO at R1: (2.5,2.5).....	67
Figure 4.10 BER versus $P_T^{\text{total}}$ for tilting polar angles of PDs for 4×4- and 9×4-MIMO at R2:(1,1).....	67

## LIST OF FIGURES (Continued)

	Page
Figure 4.11 BER versus polar angle of 4×4- and 9×4-MIMO systems with $P_T^{\text{total}} = 30$ dBm and $P_T^{\text{total}} = 27$ dBm at R1: (2.5,2.5).....	68
Figure 4.12 BER versus polar angle of 4×4- and 9×4-MIMO systems with $P_T^{\text{total}} = 30$ dBm and $P_T^{\text{total}} = 27$ dBm at R2: (1,1).....	69
Figure 4.13 Bird's eye view of LED transmitter locations for (a) scenarios with 4 transmitters, (b) scenarios with 6 transmitters, and (c) scenarios with 8 transmitters.....	74
Figure 4.14 Bird's eye view of user locations shown as digits and transmitter locations shown as dots (a) scenario 1, (b) scenario 2.....	75
Figure 4.15 Average minimum user throughputs for scenarios with $M_t = 4, K = 4$ , and $M_r' = 2$ .....	78
Figure 4.16 Average minimum user throughputs for scenarios with $M_t = 6, K = 6$ , and $M_r' = 2$ .....	79
Figure 4.17 Average minimum user throughputs for scenarios with $M_t = 8, K = 8$ , and $M_r' = 2$ .....	80
Figure 4.18 Average minimum user throughputs for scenarios with $M_t = 8, K = 4$ , and $M_r' = 2$ .....	83

# CHAPTER 1

## INTRODUCTION

### 1.1 Rationale and Problem Statement

Recently, there is an increasing demand of users to access high-speed data transmissions in wireline and wireless communications. With the access network technologies such as coaxial cable, optical fiber and radio frequency (RF), there are one or multiple limitations in terms of narrow bandwidths, low data rates, spectrum licensing fees, security issues, expensive devices and high costs of installations (Goldsmith, 2005; Medleh et al., 2011). Therefore, optical wireless communications (OWC) technology, which is an alternative for the current wireless RF solutions, has been explored. In approximately 1200 BC, OWC was first used to transmit a message for wireless communications. In recent years, it has been gaining attention in research communities as well as in industry since OWC systems offer certain advantages over RF systems. For example, OWC can provide a wide bandwidth within a license-free frequency band up to THz in the wavelength range of 700 – 1500 nm. It has a low cost of development and ease of installation. In addition, OWC has higher security than RF communications since it is very difficult to intercept optical signals from outside the room. In practical indoor OWC systems, light emitting diode (LED) and laser diode (LD) are currently used in commercial applications. Due to health hazard issues, most OWC systems to date have considered LEDs as transmitters. In addition, LEDs can be used to transmit information together with illumination at the same time because of their fast switching capabilities compared to traditional incandescent and fluorescent sources. Nevertheless, since the modulation bandwidth of LED is limited,



i.e., 20 MHz for white LED, it is challenging to achieve high-speed data transmissions in OWC systems (Kahn and Barry, 1997; Komine and Nakagawa, 2004; Tanaka et al., 2003; Elgala et al., 2007; Elgala et al., 2009; Ghassemlooy et al., 2017).

To overcome the bandwidth limitation, orthogonal frequency division multiplexing (OFDM) has been proposed to further enhance the data rates and increase the bandwidth efficiency (Armstrong, 2009; Mesleh et al., 2011; Xia et al., 2012). Consider an LED which is a non-coherent light source. The transmit optical signal is modulated in terms of light intensity and received by a photo diode (PD), which is referred to as intensity modulation and direct detection (IM/DD). To integrate OFDM with OWC, the transmit signals have to be real and non-negative. The real signal values can be obtained by using the Hermitian symmetry property. To create non-negative signal values, there are a few known non-negative OFDM transmission techniques called DC bias optical OFDM (DCO-OFDM), asymmetrically clipped optical OFDM (ACO-OFDM) and flip-OFDM. According to (Armstrong and Lowery, 2006; Armstrong and Schmidt, 2008; Fernando et al., 2011; Fernando et al., 2012), ACO-OFDM and flip-OFDM provide higher power efficiency than DCO-OFDM. In addition, flip-OFDM provides the same power efficiency and spectral efficiency as ACO-OFDM. Moreover, flip-OFDM requires less computation (Dissanayake and Armstrong, 2013; Fernando et al., 2011; Fernando et al., 2012). This thesis considers flip-OFDM for indoor OWC transmission systems.

Additionally, to further improve transmission performances, one of the most widely used techniques in modern communication systems is to increase the number of transmit and receive antennas, which is known as the multiple-input multiple-output (MIMO) technique. MIMO can either increase the overall data rate through

spatial multiplexing gain or improve the system reliability through spatial diversity gain. The combination of MIMO and OFDM has been proposed in RF communication systems and applied in several standards (Goldsmith, 2005; Bolcskei, 2006; Fath and Haas, 2013; Pathak et al., 2015). On the other hand, to boost the data rate in OWC scenarios, the MIMO technique has been considered by using multiple LED light sources together with multiple receivers. However, the MIMO-OWC system performances are limited because of the strong correlation among propagation paths. To mitigate such effects, there have been several studies on the receiver front-end designs of MIMO-OFDM in indoor OWC scenarios to reduce MIMO channel correlation in OWC (Kumar and Jeyachitra., 2019; Burton et al., 2014; Wang et al., 2015; He et al., 2015; He et al., 2016; Hong et al., 2016; Wang et al., 2017). For example, non-imaging receivers based on prism arrays were demonstrated in MIMO OWC systems (Wang et al., 2015). The demonstration showed that even through the non-imaging receiver provides a compact planar structure, a large field of view (FOV) and a well-conditioned MIMO channel matrix, it suffers from high power losses. In addition, an alternative approach is to use an aperture-based receiver, but it requires additional hardware with higher complexity (Wang et al., 2015; He et al., 2015; Wang et al., 2017). Finally, when low-cost PDs are used, it is necessary to have good alignment between transmitters and receivers due to narrow FOVs.

Unlike the RF counterparts, indoor OWC channels are typically dominated by line-of-sight (LOS) components, where MIMO channel matrix does not provide a rich scattering environment. This practically results in a single spatial channel from an ill-conditioned matrix (effectively of rank 1). This lack of spatial channels in MIMO OWC systems makes it difficult to exploit spatial multiplexing to support high data

rates. One solution for this problem is to use the singular value decomposition (SVD) precoding method when the channel state information (CSI) is available at both transmitter and receiver (Goldsmith, 2005). Several studies on SVD-based MIMO OWC systems have been reported (Hong et al., 2013; Hong et al., 2016; Ying et al., 2015; Butala et al., 2013; Park et al., 2011; Liu et al., 2014) with a focus on system performance improvement by utilizing the angular diversity of receiver PDs.

In addition, it is also possible to further improve the system capacity by apply the bit loading algorithm (Goldsmith, 2005; Iwaizumi et al., 2012; Iwaizumi et al., 2013).

To the best of the author's knowledge, the effects of LED transmitter distribution on the performance of SVD-based MIMO-OFDM OWC has not been investigated. Therefore, to further improve the system performance measured in terms of the bit error rate (BER), this research considers LED transmitter distribution in addition to angular diversity based on tilting receiver PDs. In the first half of the thesis, the research studies the performance of indoor SVD-based MIMO-OFDM OWC systems. In addition, since SVD decomposes the MIMO channel into parallel sub-channels with different path losses, the bit loading technique is utilized.

To utilize the OWC broadcast nature, multiple-user systems are considered. To extend the use of MIMO transmissions for high data rate communications, multi-user MIMO-OWC (MU-MIMO-OWC) systems have been investigated. In the case of MU-MIMO-OWC system with spatial multiplexing (SMP), multiple LEDs simultaneously transmit multiple data streams to multiple users at different locations resulting in multi-user interference (MUI), which has adverse effects on the transmission performance at each user's receiver. Based on this, the ideas of MUI mitigation by linear and non-linear precoding schemes have been proposed for RF

systems, and were applied in MU-MIMO-OWC to cancel MUI such as dirty paper coding (DPC), zero-forcing (ZF) precoding, and block diagonalization (BD) precoding (Pathak et al., 2015; Al-Ahmadi et al., 2018). Among them, DPC can achieve the maximum sum rate in MU-MIMO broadcast channels. However, DPC is difficult to implement in practice due to the complexity of nonlinear signal processing. Another method used to reduce the computation complexity of DPC is ZF-based linear precoding approaches. It is commonly used to achieve the diversity gain in MIMO broadcast communications. ZF is employed to prevent interference among all data streams transmitted from multiple LEDs, even among the data streams going to the same user. However, it amplifies noise at the receivers, yielding performance degradation (Wang et al., 2015; Wang et al., 2015; He et al., 2015; Wang et al., 2017).

Alternately, BD is considered as a compromise, which supports multiple data stream transmissions and eliminates the MUI regardless of the noise. In addition, BD is proposed to improve the sum capacity or reduce the transmitted power (Khan et al., 2014). Unlike ZF precoding, BD precoding prevents interference among individual users only. To further prevent the interference among individual data streams of each user, SVD is required. As a result, BD precoding does not suffer from noise amplification as much as ZF precoding. In general, SVD based MIMO systems have been widely investigated in RF communications where SVD is normally used to decompose the MIMO channel into a number of unequally weighted independent subchannels that are equivalent to multiple single-input single-output (SISO) channels. Hence, it is possible to eliminate the interchannel interference. However, BD precoding is not applicable when the number of PDs exceeds the number of LED transmitters. Therefore, several exiting works assumed that the total number of PDs at

all user's receivers does not exceed the number of LEDs (Hong et al., 2013; Chen et al., 2014; Marshoud et al., 2015; Pham et al., 2015; Jha et al., 2017; Zeng and Du., 2017; Zhao et al., 2017; Zhao et al., 2020).

In the second half of the thesis, the research considers a lot of user devices in the same room, yielding more PDs than LEDs. To overcome the limitation of BD precoding, user grouping is performed, and time division multiplexing (TDM) is applied with BD precoding for each user group. For example, with four LED transmitters and four users each with two PDs, the users can be divided into two groups of two users and TDM is then used with BD precoding applied in each timeslot.

## 1.2 Research Questions

The research focuses on MIMO-OWC systems based on IM/DD where the LOS components dominate, yielding lack of spatial channels. The main challenge is to exploit spatial multiplexing to support high data rates. The research questions are divided into two parts.

The first part considers single-user MIMO-OWC systems. Here, the question is how to break the symmetry of the arrangement between transmitters and receivers in MIMO-OWC systems in order to avoid ill-conditioned MIMO channel matrices under the impact of the OFDM symbol design, the configuration of MIMO transmitters, the required data rate, the available BW, and the angular diversity based on tilting receiver PDs.

The second part focuses on multiuser MIMO-OWC systems where it is possible to have more photo detectors at all the receivers than the number of LEDs at

the transmitter. The question is how to group the users in a MU-MIMO OWC system with BD precoding so that the transmission performance is maximized. For fairness, the goal is to maximize the minimum user throughput.

### 1.3 Research Aims

The research provides the following contributions on SVD-based MIMO-OFDM OWC systems.

1. This research investigates the BER performances of MIMO flip-OFDM transmissions for indoor OWC using SVD through mathematical analysis as well as simulation experiments whose results are validated through a close match.
2. This research demonstrates the performances of MIMO flip-OFDM using SVD through bit loading for different number of LED distributions.
3. This research investigates the optimal MIMO-OFDM system designed in terms of the operating bandwidth for a fixed BER requirement.
4. This research evaluates the effects of varying the tilting polar angle of the receive PDs under various transmit optical power levels (light dimming).

Next, the main objectives of MU-MIMO OWC based on BD systems are listed below.

5. This research performs efficient user grouping by applying time division multiplexing (TDM) with BD precoding.
6. This research investigates the user throughput with different grouping heuristics.

#### 1.4 Scopes and Limitations

For the purpose of performance optimization of indoor SVD-based MIMO-OFDM OWC systems, the scopes and limitations are shown below.

1. The numerical results of this research's scenario are obtained from analytical derivations and computer simulations using the MATLAB software.
2. The multi-carrier modulation method is based on flip-OFDM.
3. The three different MIMO OWC configurations include  $4 \times 4$ ,  $9 \times 4$  and  $16 \times 4$ .
4. The optical channel is considered as LOS with Lambertian emission patterns from LEDs.

#### 1.5 Research Outlines

In chapter 1, the rationale and problem statement of the research are described followed by research questions, research aims, scopes and limitations, respectively. Chapter 2 contains the literature reviews of OWC, OFDM, OFDM for OWC, MIMO, MIMO OFDM using SVD, MU-MIMO in OWC, and BD precoding for MU-MIMO in OWC. Chapter 3 shows the research methodology which is divided into two scenarios. The first scenario considers the configuration system of single-user MIMO and the mathematical analysis on the performance optimization of indoor SVD-based MIMO-OFDM OWC systems. Next, the second scenario considers the system configuration and system model of MU-MIMO, and efficient user grouping for MU-MIMO OWC based on BD. In chapter 4, the simulation results of both scenarios are presented. Then, chapter 5 presents research conclusions and recommendations.

## CHAPTER 2

### LITERATURE REVIEW

#### 2.1 Overview of OWC

Nowadays, there is an increasingly large number of smartphones, tablets, and other electronic devices that require access to high-speed data transmissions, which play an important role in people's lives. On the other hand, the RF bandwidth is a scarce and/or licensed resource which is unable to satisfy the high bandwidth demands in the future. Therefore, an alternative wireless transmission called OWC has been explored. OWC becomes an emerging complement to RF communications with several outstanding advantages. For instance, the OWC spectrum is an unlimited and unregulated frequency band. Optical signals provide high security from eavesdropping and prevent interference between rooms or buildings. In addition, optical signals are immune to electromagnetic interference.

White LEDs are commonly used for illumination for both indoor and outdoor applications due to their low energy consumption compared to fluorescent lamps and incandescent lamps. Moreover, due to the fast response of LEDs, they are able to support communication and illumination at the same time. Furthermore, LEDs are known to be environmental friendly. However, there are some health risks caused by LEDs' flicker frequencies, brightness and other factors that may induce biological human responses such as seizures, malaise, headaches and eyestrain (Wilkins et al, 2010). Even though the available visible light bandwidth is up to several THz, the bandwidth of OWC is limited at several MHz due to the limited modulation bandwidth of LEDs.



OWC systems using white LEDs are referred to as visible light communications (VLC). VLC was initially proposed by (Tanaka et al., 2003) and has been investigated by many researches (Komine and Nakagawa, 2004; Afgani et al., 2006; Elgala et al., 2007; Elgala et al., 2009; Wilkins et al., 2010; Matheus et al., 2019). Currently, VLC has been standardized for short-range OWC proposed by Institute of Electrical and Electronics Engineers (IEEE) as IEEE 802.15.7 in 2011 and 2018 (IEEE, 2011; IEEE, 2018). In addition, there are three Japanese standards of VLC proposed by Japan Electronics and Information Technology Industries Association (JEITA), including VLC system standard (JEITA CP-1221), visible light ID system standard (JEITA CP-1222) and visible light beacon standard (JEITA CP-1223) (jeita.or.jp).

In a typical indoor environment, besides LEDs, LDs can be used as light sources, and PDs are used as detectors. With power detection, the transmit optical signals have to satisfy the IM/DD property where data bits are transmitted in terms of optical intensity and received through power detection (Kahn and Barry, 1997). In general, OWC channel impulse responses consist of two components from LOS propagation and diffuse propagation. According to (He et al., 2015; He et al., 2016), the LOS component is typically much stronger than the diffuse component. This thesis assumes OWC links with LOS characteristics. Figure 2.1 illustrates a LOS propagation model. As shown in the figure,  $\vartheta_T$  is the angle of emission with respect to the transmitter (Tx) and  $\varphi_R$  is the angle of incidence with respect to the receiver (Rx).

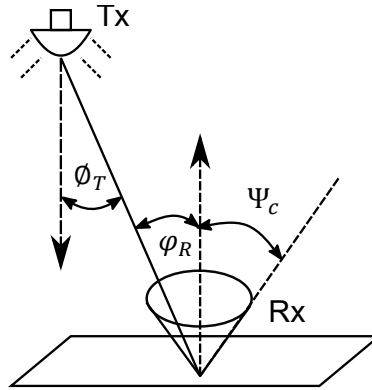


Figure 2.1: LOS propagation model

For an OWC link with Lambertian LEDs, the channel gain of the OWC link between an LED and a PD can be calculated using (Wu et al., 2016)

$$h = \begin{cases} \frac{(m+1)A}{2\pi d^2} \cos^m(\phi_T) \cos(\phi_R), & 0 \leq \phi_R \leq \Psi_{\text{FOV}} \\ 0, & \phi_R \geq \Psi_{\text{FOV}} \end{cases} \quad (2.1)$$

where  $h$  is the gain from the LED to the PD,

$A$  is the PD collection area,

$m$  is the Lambertian order,

$d$  is the distance between the LED to the PD,

$\Psi_{\text{FOV}}$  is the FOV of the PD with  $\Psi_{\text{FOV}} \leq \pi/2$ ,

$\phi_T$  is the emission angle at the transmit LED,

$\phi_R$  is the incident angle at the receive PD.

## 2.2 Overview of OFDM

OFDM has been proposed to achieve high data rates using frequency-selective channels and improve the spectral efficiency of traditional frequency division multiplexing (FDM). It was proposed in 1996 by Chang of Bell Labs

(Armstrong, 2009). Nowadays, OFDM is applied extensively in wired and wireless communication systems such as Wi-Fi, WiMAX, 3G, LTE, digital TV, and so on (Armstrong, 2009). OFDM is a multicarrier modulation technique where the allocated bandwidth of OFDM is divided into a number of smaller frequency bands called subcarriers. Each subcarrier is modulated with one of several digital modulation schemes, such as binary phase shift keying (BPSK), quaternary phase shift keying (QPSK), 16- and 64-QAM, etc., at a lower data rate. These lower-rate streams are transmitted in parallel over a number of subcarriers, unlike single-carrier modulation techniques in which a high-rate serial data stream is modulated over a single carrier within the bandwidth, as shown in Figure 2.2. This results in a longer symbol period for multicarrier transmission, and here the intersymbol interference (ISI) effect is mitigated. That is why OFDM is more robust to ISI for transmissions over a dispersive channel (Goldsmith, 2005; Proakis and Salehi, 2008; Armstrong, 2009).

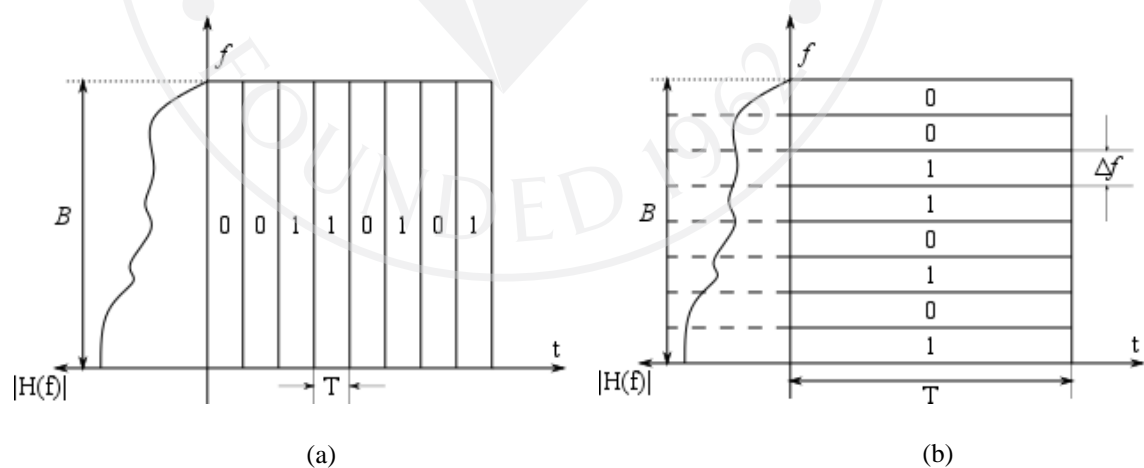


Figure 2.2: (a) single-carrier transmission and (b) multicarrier transmission

Figure 2.3 shows the bandwidth efficiency of OFDM compared to the basic FDM scheme. Although, the concept of OFDM is based on FDM, OFDM can save almost 50% of the utilized bandwidth since OFDM subcarriers are orthogonal to one

another despite their overlapping frequency spectra and the use of a guard interval (GI) in terms of the cyclic prefix (CP) to minimize ISI. Therefore, the data rate of OFDM is increased using same bandwidth.

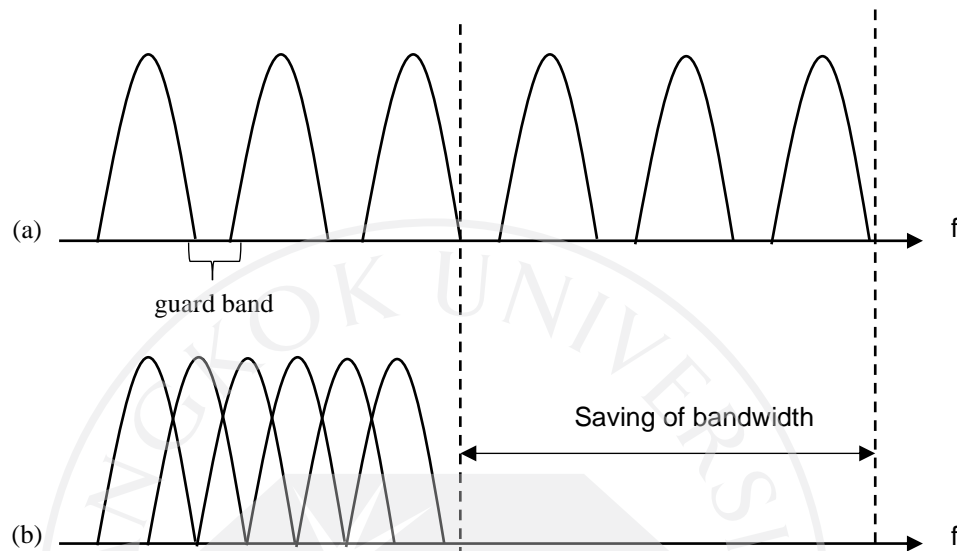


Figure 2.3: Spectra of (a) FDM carriers and (b) OFDM subcarriers

The orthogonality property of transmitted signals on subcarriers is described mathematically in (2.2), where the orthogonality of two signals means that

$$\int s_n(t)s_k^*(t)dt = 0, \quad n \neq k \quad (2.2)$$

where  $s_n(t)$  presents the transmit signal on subcarrier  $n$ ,

$s_k(t)$  presents the transmit signal on subcarrier  $k$ .

In addition, without using extremely complex signal processing for a large number of subcarriers involving oscillators and filters at transmitters and receivers, OFDM modulation and demodulation can be performed by using (IDFT) and discrete Fourier transform (DFT). Let  $S_0, \dots, S_{N-1}$  be the QAM symbols to be transmitted on subcarriers  $0, \dots, N - 1$ , and  $s_0, \dots, s_{N-1}$  be the IDFT results obtained from

$S_0, \dots, S_{N-1}$ . According to (Proakis and Salehi, 2008), IDFT and DFT operations can be expressed as follows.

$$s_n = \frac{1}{\sqrt{N}} \sum_{k=0}^{N-1} S_k e^{i2\pi kn/N}, n \in \{0, \dots, N-1\} \quad (2.3)$$

$$S_k = \frac{1}{\sqrt{N}} \sum_{n=0}^{N-1} s_n e^{-i2\pi kn/N}, k \in \{0, \dots, N-1\} \quad (2.4)$$

A basic OFDM architecture with the CP insertion is given in Figure 2.4. Data bits are modulated by a QAM modulator yielding a QAM symbol  $S_k$  carried on subcarrier  $k \in \{0, \dots, N-1\}$  in the frequency domain. Then, IDFT produces  $N$  signal values in the time domain. In the time domain, the CP of length  $N_{CP}$  is inserted between successive OFDM symbols to prevent ISI at the receiver caused by multipath delay spread in the channel. At the receiver, DFT is performed on each  $N$ -subcarrier OFDM symbol. Then, a simple equalizer, called one-tap equalizer, is used to compensate the subcarrier gains. Finally, a QAM demodulator recovers the original data bits on each subcarrier.

### 2.3 Overview of OFDM for OWC

Over two decades, OFDM has been widely adopted for optical communication due to its many advantages demonstrated in RF communications. Recently, there is an increasing number of papers on the study of OFDM for indoor OWC through visible light since white LEDs have limited modulation bandwidths, making OWC channels frequency-selective at high data rates. To support OFDM for VLC based on LEDs,

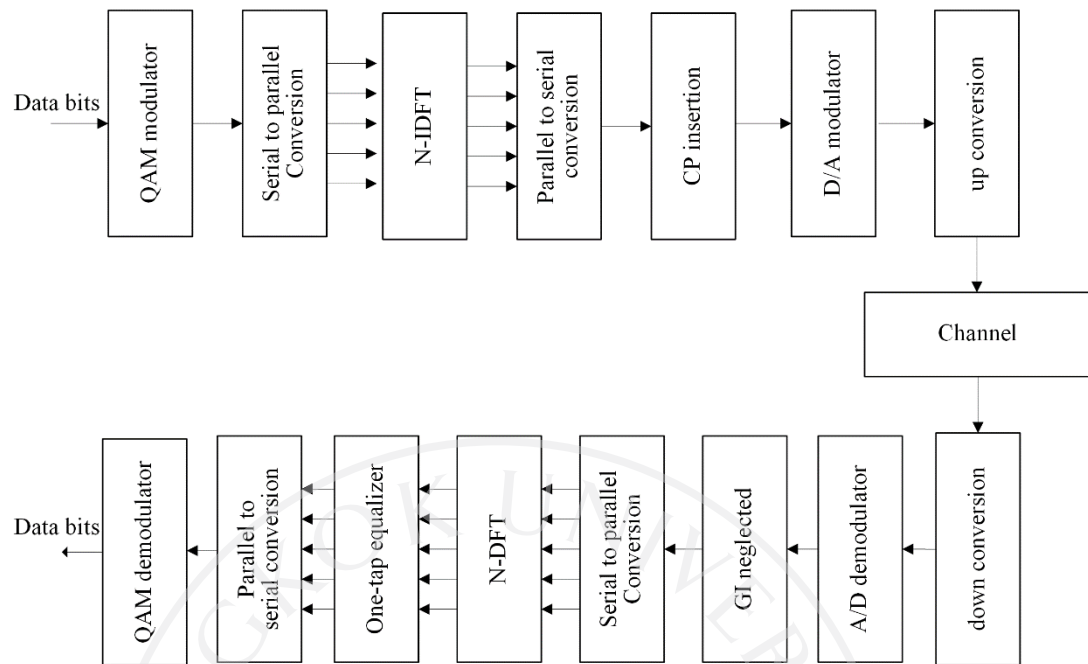


Figure 2.4: OFDM transmission system diagram

the transmitted and received signals are expected to be processed by IM/DD, and must therefore be real and non-negative. To satisfy these requirements, a real OFDM signal is first created using the Hermitian symmetry property defined as follows.

$$S_0 = S_{N/2} = 0 \quad (2.5)$$

$$S_{N-k} = S_k^*, k = \{1, \dots, N/2 - 1\} \quad (2.6)$$

Next, to make the OFDM signals non-negative, a few techniques have been proposed including DCO-OFDM, ACO-OFDM and flip-OFDM (Armstrong and Lowery, 2006; Armstrong and Schmidt, 2008; Fernando et al., 2011; Fernando et al., 2012; Dissanayake and Armstrong, 2013). The details of each technique to obtain non-negative OFDM signals can be described as follows.

- DCO-OFDM: A constant DC value is added to the transmitted OFDM signals.

Both odd- and even-numbered subcarriers are used to carry data. A drawback

of DCO-OFDM is high transmit optical power when a large DC bias is added.

It is considered inefficient in terms of optical power.

- ACO-OFDM: Without DC bias, all negative signal values are clipped to be zero. ACO-OFDM carries data only on the odd-numbered subcarriers whereas the even-numbered subcarriers contain the signal distortion due to negative clipping.
- Flip-OFDM: Without DC bias, all negative signal values from both odd- and even-numbered subcarriers are clipped to be zero. However, flip-OFDM uses two-subframes where the first subframe carries the original OFDM signals, to be followed by the second subframe with the negative or flipped OFDM signals.

According to (Armstrong and Schmidt, 2008; Fernando et al, 2011;

Dissanayake and Armstrong, 2013), the authors have investigated the power efficiency and the spectral efficiency of DCO-OFDM, ACO-OFDM and flip-OFDM.

It can be concluded as follows.

- ACO-OFDM and flip-OFDM provide better power efficiency than DCO-OFDM since they do not need the DC bias, which increases in the transmit optical power.
- ACO-OFDM and flip-OFDM have the same power efficiency and spectral efficiency, but flip-OFDM requires less computation.

Moreover, OFDM is more power efficient than on-off-keying (OOK) and pulse position modulation (PPM), as pointed out in (Armstrong and Schmidt, 2008; Dissanayake and Armstrong, 2013). This thesis focuses on flip-OFDM transmissions only.

### 2.3.1 Fundamentals of Flip-OFDM transmission system

There are  $N/2 - 1$  independent QAM symbols carried on both odd- and even-numbered subcarriers. For each OFDM symbol, flip-OFDM signal values are separated into two consecutive subframes. The first subframe carries the original OFDM signals, and the second subframe carries the negative OFDM signals. Figure 2.5 shows the flip-OFDM transmission for OWC. A flip-OFDM transmission system is based on conventional OFDM transmissions but contains some special blocks to create real OFDM signals and to make non-negative signals, as indicated by the block diagrams with dashed lines. Since data are carried on two subframes, there are  $2(N + N_{CP})$  signal values transmitted per flip-OFDM symbol. Let  $s'_n$  and  $-s'_n$  denotes the first subframe (original OFDM signal) and the second subframe (negative of the original OFDM signal) of  $s_n$ , respectively. Then the combination of two subframes with the CP can be expressed as

$$s'_{N-N_{CP}}, \dots, s'_{N-1}, s'_0, \dots, s'_{N-1}, -s'_{N-N_{CP}}, \dots, -s'_{N-1}, -s'_0, \dots, -s'_{N-1} \quad (2.7)$$

From the above expression, the non-negative signals can be obtained by negative clipping.



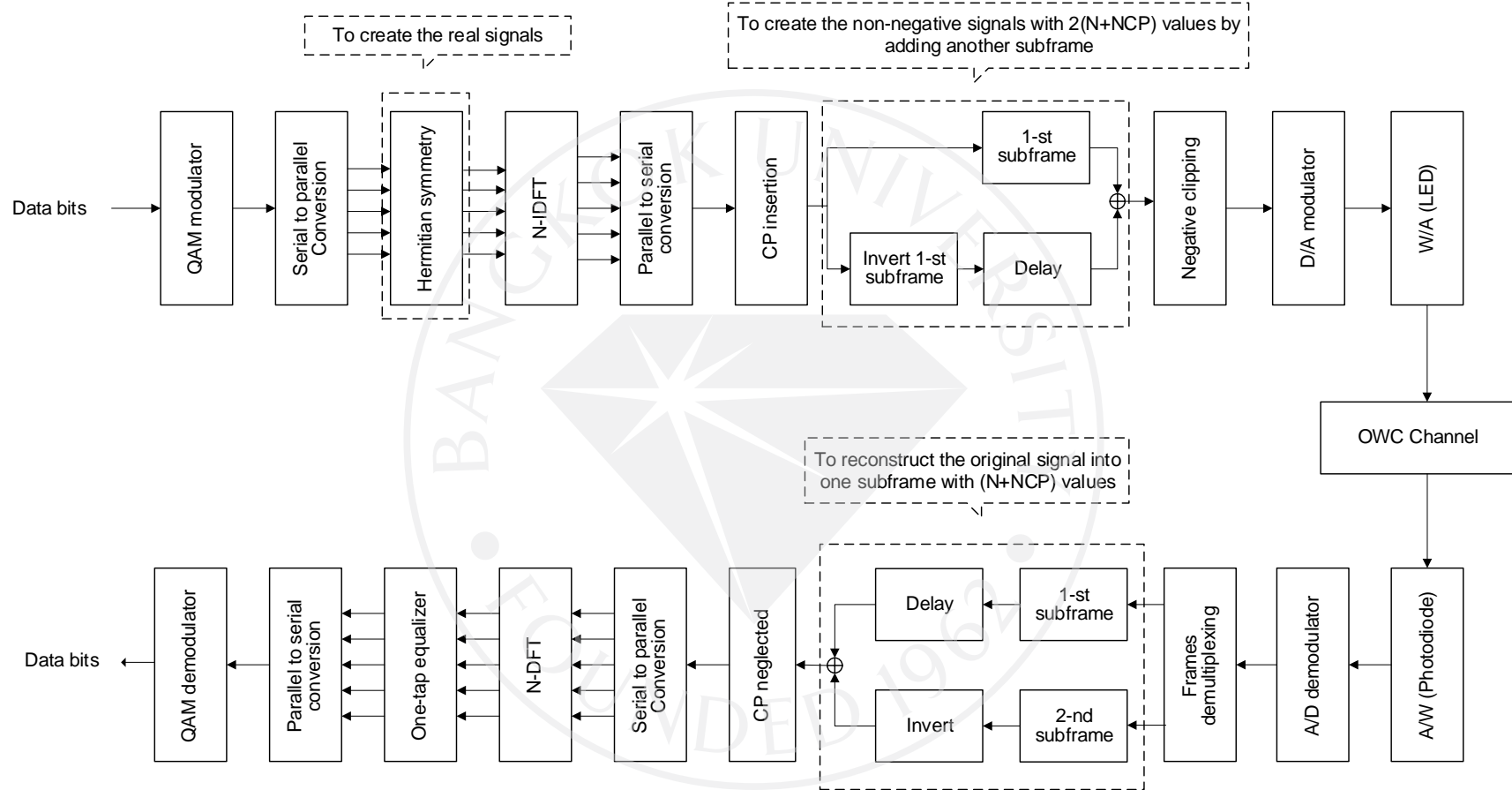


Figure 2.5: Flip-OFDM transmission system diagram

## 2.4 Overview of MIMO

The MIMO technique was pioneered by Winter in 1987 (Goldsmith, 2005; Pathak et al., 2015). Compared to the traditional SISO systems, MIMO is now increasingly used to enhance link capacities and/or offer high link reliability on RF wireless communications such as WiFi, WiMAX, 3G, and LTE. Basically, MIMO can support spatial diversity or spatial multiplexing. It uses separate antennas, which are located in different locations, to take advantage of different propagation paths. This can be done by using multiple antennas at both transmitter and receiver as shown in Figure 2.6.

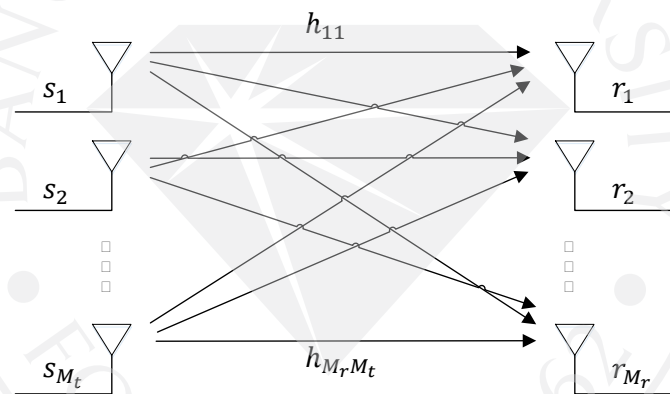


Figure 2.6: MIMO transmission system

Source: Goldsmith, 2005: 300

Figure 2.6 shows the basic transmission system of MIMO with  $M_t$  transmit and  $M_r$  receive antennas (Goldsmith, 2005). In a noiseless scenario, the system can be represented as a mathematic model as

$$\begin{bmatrix} r_1 \\ \vdots \\ r_{M_r} \end{bmatrix} = \begin{bmatrix} h_{11} & \dots & h_{1M_t} \\ \vdots & \ddots & \vdots \\ h_{M_r 1} & \dots & h_{M_r M_t} \end{bmatrix} \begin{bmatrix} s_1 \\ \vdots \\ s_{M_t} \end{bmatrix}$$

where  $s_j$  represents the transmitted signal on antenna  $j$ ,

$r_i$  represents the received signal on antenna  $i$ ,

$h_{ij}$  is the gain from transmit antenna  $j$  to receive antenna  $i$ .

Due to fluctuations of the environment, the transmit signal may get lost or so severely corrupted that the receiver cannot retrieve it. By introduction of MIMO, this problem can be mitigated by the spatial diversity technique in which the same data are transmitted across independent channels to combat fading. This makes MIMO resistant to signal degradation caused by multipath propagation.

On the other hand, under certain environments, MIMO can increase the overall data rate by the spatial multiplexing technique in which the transmit antennas send independent data streams to the receive antennas. Since all antennas operate in the same allocated bandwidth, the transmitted independent data certainly interfere with one another. To eliminate this interference, SVD, which is broadly applied on RF communications, is performed (Goldsmith, 2005; Bolcskei, 2006).

#### 2.4.1 Parallel Decomposition of the MIMO Channel

Independent parallel channel decomposition can be obtained by SVD. SVD is a general method to produce the multiplexing gain when the CSI is known at the transmitter and the receiver. By the SVD technique, the multiplexing gain is generated by decomposing the MIMO channel into a number of parallel independent channels, each of which can be thought of as a SISO channel (Goldsmith, 2005; Butala et al., 2006; Park et al., 2011; Hong et al., 2016).

In particular, the channel matrix  $\mathbf{H}_{M_r \times M_t}$  can be decomposed as

$$\mathbf{H} = \mathbf{U}\mathbf{\Sigma}\mathbf{V}^H \quad (2.8)$$

where  $\mathbf{U}_{M_r \times M_r}$  and  $\mathbf{V}_{M_t \times M_t}$  are unitary matrices, i.e.,  $\mathbf{U}^H \mathbf{U} = \mathbf{U} \mathbf{U}^H = \mathbf{I}_{M_r}$  and  $\mathbf{V}^H \mathbf{V} = \mathbf{I}_{M_t}$ , and  $\mathbf{\Sigma}_{M_r \times M_t}$  is a diagonal matrix. The diagonal elements of  $\mathbf{\Sigma}$  are the singular values of matrix  $\mathbf{H}$ , with  $\sigma_i$  denoting the  $i$ th diagonal element.

Let  $L_H$  be the rank of matrix  $\mathbf{H}$ , where  $L_H \leq \min(M_t, M_r)$ . In a rich scattering environment or uncorrelated channel,  $\mathbf{H}$  is observed to be full rank and provides an efficient multiplexing gain, which enhances the throughput up to a factor of  $L_H = \min(M_t, M_r)$ . Otherwise, in a LOS environment with a highly correlated channel matrix, the rank of  $\mathbf{H}$  is low. In the worst case, the rank of  $\mathbf{H}$  is 1. This leads to an inefficient spatial multiplexing gain where the throughput cannot be increased.

Now, consider the basics of MIMO transmission systems using SVD, which is illustrated in Figure 2.7. First, the input data stream is precoded by the unitary matrix  $\mathbf{V}$  at the transmitter, and then decoded by the unitary matrix  $\mathbf{U}^H$  at the receiver.

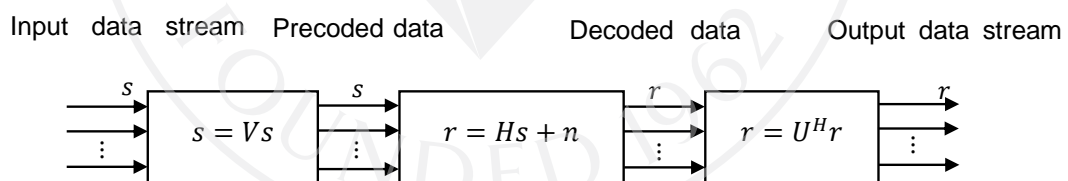


Figure 2.7: MIMO transmission system using SVD

Source: Goldsmith, 2005: 301

The received output data stream  $\tilde{\mathbf{r}}$  after decoding can be written as

$$\begin{aligned} \tilde{\mathbf{r}} &= \mathbf{U}^H \mathbf{r} \\ &= \mathbf{U}^H (\mathbf{H} \mathbf{s} + \mathbf{n}) \\ &= \mathbf{U}^H (\mathbf{U} \mathbf{\Sigma} \mathbf{V}^H \mathbf{s} + \mathbf{n}) \end{aligned}$$

$$\begin{aligned}
&= \mathbf{U}^H (\mathbf{U} \mathbf{\Sigma} \mathbf{V}^H \mathbf{V} \tilde{\mathbf{s}} + \mathbf{n}) \\
&= \mathbf{U}^H \mathbf{U} \mathbf{\Sigma} \mathbf{V}^H \mathbf{V} \tilde{\mathbf{s}} + \mathbf{U}^H \mathbf{n} \\
&= \mathbf{\Sigma} \tilde{\mathbf{s}} + \mathbf{U}^H \mathbf{n} \\
&= \mathbf{\Sigma} \tilde{\mathbf{s}} + \tilde{\mathbf{n}}
\end{aligned}$$

Hence, the received data stream is  $\tilde{\mathbf{r}} = \mathbf{\Sigma} \tilde{\mathbf{s}} + \tilde{\mathbf{n}}$ , where  $\mathbf{n}$  is AWGN and  $\tilde{\mathbf{n}} = \mathbf{U}^H \mathbf{n}$  is also AWGN since  $\mathbf{U}$  is unitary. This can be explained in the matrix form as follows. Assume that  $L_H = M_t = M_r$ .

$$\begin{bmatrix} \tilde{r}_1 \\ \tilde{r}_2 \\ \vdots \\ \tilde{r}_{M_r} \end{bmatrix} = \begin{bmatrix} \sigma_1 & 0 & \dots & 0 \\ 0 & \sigma_2 & \dots & 0 \\ \vdots & \vdots & \ddots & \vdots \\ 0 & 0 & 0 & \sigma_{M_t} \end{bmatrix} \begin{bmatrix} \tilde{s}_1 \\ \tilde{s}_2 \\ \vdots \\ \tilde{s}_{M_t} \end{bmatrix} + \begin{bmatrix} \tilde{n}_1 \\ \tilde{n}_2 \\ \vdots \\ \tilde{n}_{M_r} \end{bmatrix}$$

From the above equation, the matrix  $\mathbf{\Sigma}$  is a diagonal matrix of singular values of  $\mathbf{H}$ . It provides parallel independent channels that do not interfere with one another. More specifically,

$$\begin{aligned}
\tilde{r}_1 &= \sigma_1 \tilde{s}_1 + \tilde{n}_1 \\
&\vdots \\
\tilde{r}_{M_r} &= \sigma_{M_t} \tilde{s}_{M_t} + \tilde{n}_{M_r}
\end{aligned}$$

To sum up, the data rate increases with the number  $L_H$  of parallel independent channels. This increase in the total data rate is called the multiplexing gain.

## 2.5 MIMO OFDM using SVD

The basic structure of MIMO OFDM transmission systems using SVD can be shown in Figure 2.8 and Figure 2.9. Here, the transmit signal is bipolar since it is carried on RF carrier signals. Assume that CSI is known at both transmitter and

receiver. Figure 2.8 shows the transmitter side where the data bits are modulated by a QAM modulator. Next, a serial stream of QAM symbols are converted into parallel streams by S/P conversion. These parallel streams of symbols are then multiplied with the corresponding precoding matrix obtained from SVD of the channel matrix. After that, IDFT, parallel-to-serial (P/S) conversion, and CP insertion are performed to obtain time-domain signals. The CP is usually added to the header of each OFDM symbol before transmission to prevent ISI and ICI due to multipath effects. Finally, the transmitted digital signals are transformed to analog signals by digital-to-analog (D/A) modulators. Then, the D/A outputs are transmitted through the RF channel after RF upconversion (Hong et al., 2016).

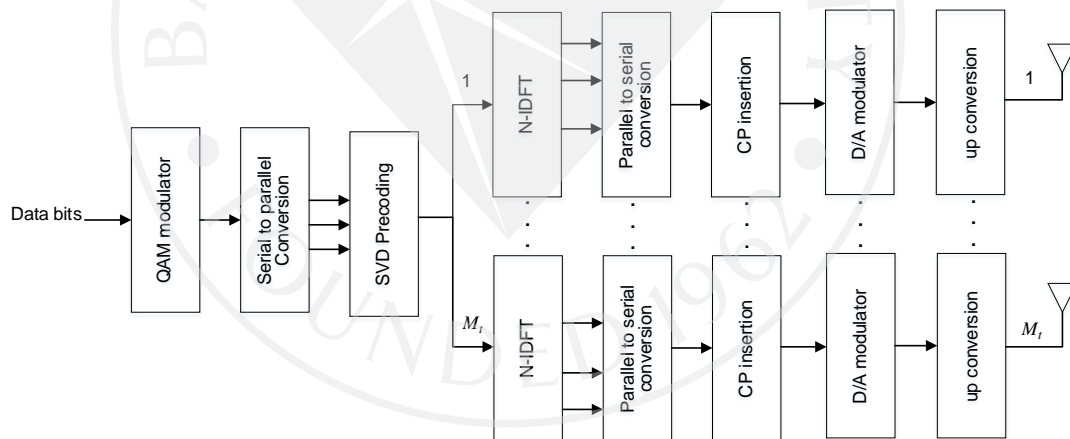


Figure 2.8: The structure of MIMO OFDM transmitter using SVD

At the receiver side, the signal processing is the inverse process of the transmitter side. The overall signal processing is presented as Figure 2.9 (Hong et al., 2016). The received signals from each receiving antenna are processed by an RF down-converter, an analog-to-digital (A/D) demodulator, CP removal, S/P

conversion and DFT to create frequency-domain signals. Then, these signals are combined by the corresponding decoding matrix of SVD. Finally, data bits are detected from the received signals by a QAM demodulator.

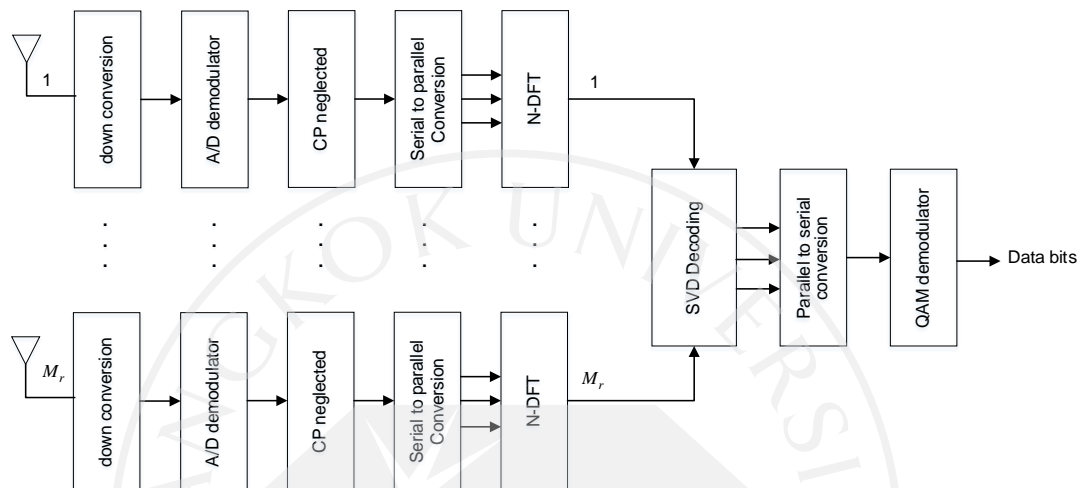


Figure 2.9: The structure of MIMO OFDM receiver using SVD

## 2.6 MU-MIMO in OWC

Multi-user MIMO (MU-MIMO) systems have been investigated over the past decade. MU-MIMO refers to communications between a wireless base station and multiple user terminals as shown in Figure 2.10. Based on traditional RF communication systems, there are two different multiuser channels: the uplink channel or the MIMO multiple access channel (MAC) and the downlink or the MIMO broadcast channel (BC). Most of the existing work concerns achieving the capacity of the MU-MIMO-BC transmission system. In the BC, there is one transmitter sending different and independent data streams to multiple receivers. The applications of BC include radio transmission systems, television systems, and downlink satellite systems. In multi-user communications, the system resources such as power and

bandwidth must be shared among the users. A efficient multiple access scheme is adopted to support multiple users simultaneously. Methods to divide the signal bandwidth include frequency division multiplexing, time division multiplexing, code division multiplexing, and hybrid methods (Goldsmith, 2005; Chen et al. 2013; Maha and Kosai, 2013; Hong et al. 2013; Al-Ahmadi et al. 2018; ).

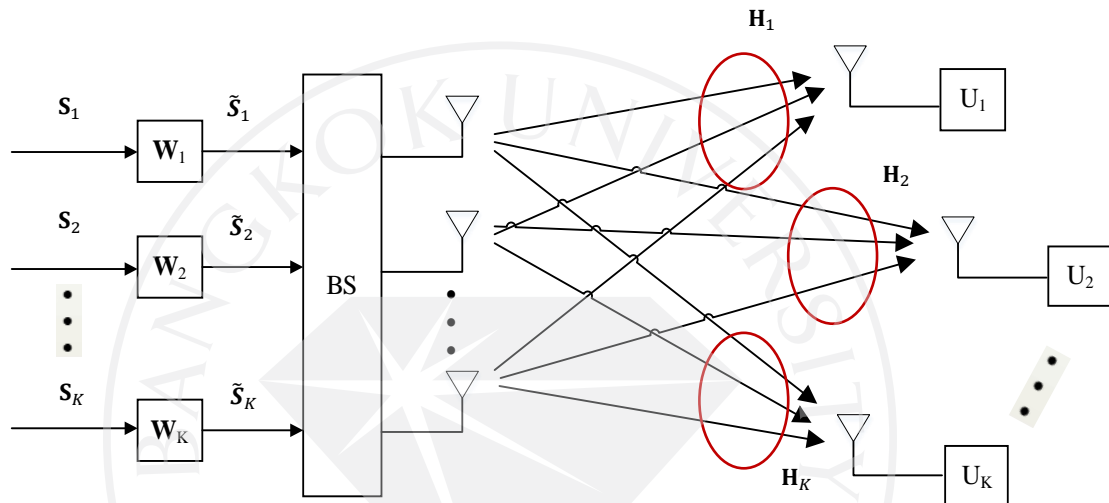


Figure 2.10: The structure of a MU-MIMO broadcasting system

Nowadays, there have been studies and development of MU-MIMO in OWC systems to satisfy the increasing demands for high data rates. A typical indoor downlink transmission system of a multi-user OWC system can be modeled as shown in Figure 2.10, where a set of LED transmitters communicate with a set of users. In particular, the  $M_t$ -LED transmitter on the ceiling transmits downlink data streams to  $K$  users, where each user is equipped with  $M'_r$  PDs. Thus, the total number of PDs at all user terminals in the OWC system is equal to  $M_r = KM'_r$ . The receiver signals at the PDs of user  $k$  is given by



$$\mathbf{r}_k = \mathbf{H}_k \mathbf{w}_k \mathbf{s}_k + \mathbf{H}_k \sum_{i=1, i \neq k}^K \mathbf{w}_i \mathbf{s}_i + \mathbf{n}_k \quad (2.9)$$

where  $\mathbf{r}_k$  is the  $M'_r \times 1$  received signal vector for user  $k$ ,

$\mathbf{H}_k$  is the  $M'_r \times M_t$  MIMO channel matrix between  $M_t$  transmit LEDs and  $M'_r$  PDs of user  $k$ ,

$\mathbf{w}_k$  is the  $M_t \times M'_r$  precoding matrix for user  $k$ ,

$\mathbf{s}_k$  is the  $M'_r \times 1$  vector of data symbols for user  $k$ ,

$\mathbf{n}_k$  is the  $M'_r \times 1$  noise vector for user  $k$  that contains independent and identically distributed (IID) Gaussian random variables with mean 0 and variance  $\sigma_{\text{AWGN}}^2$ .

Note that, in (2.9), the first and the second terms represent the desired signal and the multi-user interference (MUI) in the received signal of user  $k$ , respectively. In order to eliminate the MUI term, i.e.,  $\mathbf{H}_k \sum_{i=1, i \neq k}^K \mathbf{w}_i \mathbf{s}_i$ , the block diagonalization (BD) technique imposes a constraint on the precoding matrix  $\mathbf{w}_i$  of each user  $i$  to be orthogonal to the channel matrices associated with all other users (Hong et al. 2014; Chen et al. 2014; Pham et al. 2015; Wang et al. 2015). The constraint can be expressed as

$$\mathbf{H}_k \mathbf{w}_i = 0 \quad \text{for all } k \neq i \text{ and } 1 \leq i, k \leq K \quad (2.10)$$

The signal processing of BD can be operated as follows. First, the channel matrix  $\tilde{\mathbf{H}}_k$  is defined as

$$\tilde{\mathbf{H}}_k = [\mathbf{H}_1^H \dots \mathbf{H}_{k-1}^H \mathbf{H}_{k+1}^H \dots \mathbf{H}_K^H]^H \quad (2.11)$$

From (2.11),  $\tilde{\mathbf{H}}_k$  is a  $(K - 1) M_r' \times M_t$  matrix that contains all channel matrices except for user  $k$ , i.e.,  $\mathbf{H}_k$ . To satisfy the zero-interference constraint in (2.10),  $\mathbf{w}_i$  must be in the null space of  $\tilde{\mathbf{H}}_k$ . Assume that  $\tilde{\mathbf{H}}_k$  is full rank and  $L_k = \text{rank}(\tilde{\mathbf{H}}_k)$ . The SVD of  $\tilde{\mathbf{H}}_k$  can be obtained as

$$\tilde{\mathbf{H}}_k = \tilde{\mathbf{U}}_k \tilde{\Sigma}_k \tilde{\mathbf{V}}_k^H \quad (2.12)$$

where  $\tilde{\mathbf{V}}_k = [\tilde{\mathbf{V}}_k^1 \ \tilde{\mathbf{V}}_k^0]$ ,  $\tilde{\mathbf{V}}_k^1$  holds the first  $L_k$  right singular vectors corresponding to non-zero singular values, and  $\tilde{\mathbf{V}}_k^0$  contains the last  $M_r'$  columns of  $\tilde{\mathbf{V}}_k$  and is the basis matrix for the null space of  $\tilde{\mathbf{H}}_k$ . In other words, when the transmitted signals are multiple with  $\tilde{\mathbf{V}}_k^0$  before transmissions, only the user  $k$  receives the signals while all other users receive nothing.

After applying the null space  $\tilde{\mathbf{V}}_k^0$  to the channel matrix  $\mathbf{H}_k$ , user  $k$  has a non-interfering block channel  $\mathbf{H}_k \tilde{\mathbf{V}}_k^0$ . Thus, to decouple this block channel into  $L_k$  parallel sub-channels, the  $M_r' \times M_t$  equivalent channel matrix of user  $k$  is defined as  $\bar{\mathbf{H}}_k = \mathbf{H}_k \tilde{\mathbf{V}}_k^0$ , with the SVD of  $\bar{\mathbf{H}}_k = \bar{\mathbf{U}}_k \bar{\Sigma}_k \bar{\mathbf{V}}_k^H$ . Then, the BD precoding matrix for user  $k$  is the product of  $\mathbf{w}_k = \tilde{\mathbf{V}}_k^0 \bar{\mathbf{V}}_k$ . Therefore, BD precoding can prevent MUI. In addition, the interference between the PDs of the same user can be eliminated through the SVD of  $\bar{\mathbf{H}}_k$ .

## CHAPTER 3

### METHODOLOGY

This chapter presents the research methodology of two system scenarios as follows.

- The first scenario is single-user MIMO used to investigate performance optimization of indoor SVD-based MIMO-OFDM OWC systems.
- The second scenario explores multi-user MIMO and investigates efficient user grouping for MU-MIMO OWC based on block diagonalization.

#### 3.1 Single User MIMO for an Indoor OWC System

This section describes the system configuration, transmission system diagrams, the mathematical analysis, and the BER performance analysis, which involve both analysis and simulation approaches.

##### 3.1.1 System Model Configurations of Single-User MIMO

Figure 3.1 shows the configuration of the single user indoor MIMO OWC system to be used in this research. Assume a room with the dimension of  $5 \text{ m} \times 5 \text{ m} \times 2.5 \text{ m}$ . The  $M_r$  PD receivers are placed at the height of 0.8 m from the floor while the  $M_t$  LEDs are positioned at the height of 2.5 m above the floor. The receiver panel consists of four PDs, i.e.,  $M_r = 4$ . It is assumed that these four PDs are placed on the same plane. All the PDs have the same field of view (FOV) of  $70^\circ$  and the same effective area of  $1 \text{ cm}^2$ . In addition, the spacing between the PDs is equal to 1 cm. The inset shows the coordinate of the receive PD orientations.

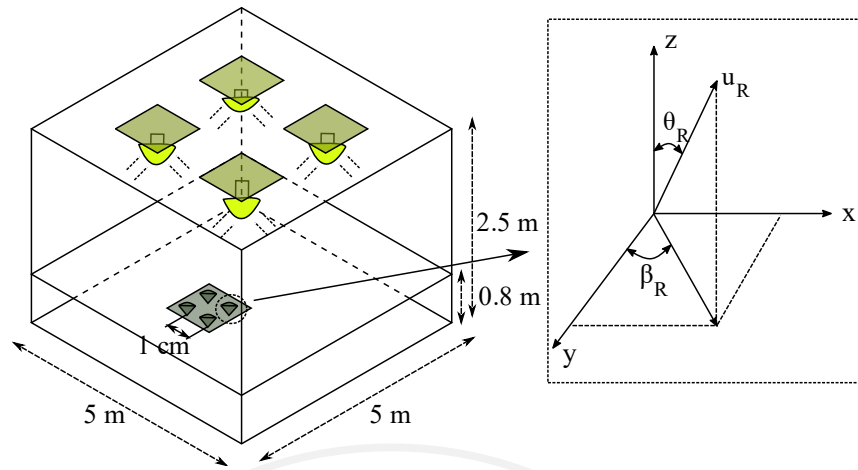


Figure 3.1: Configuration of the single user indoor MIMO OWC system and its spherical coordinates.

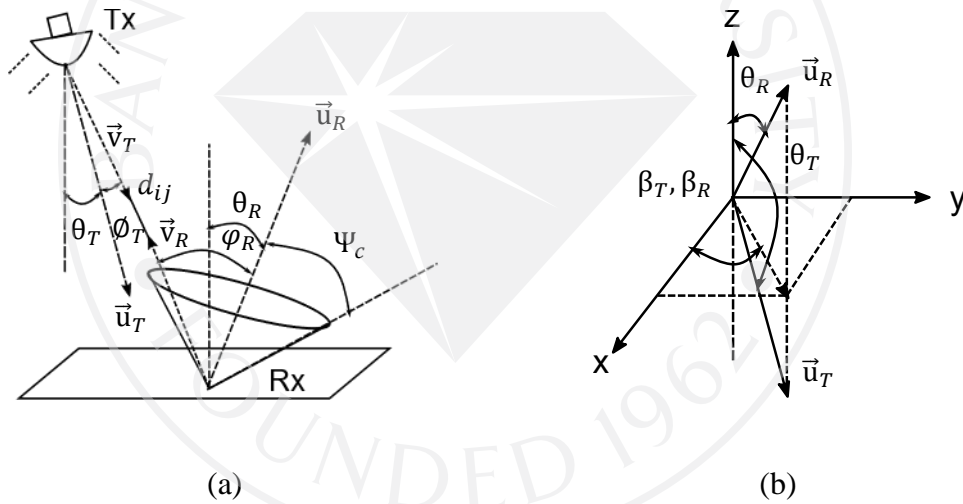


Figure 3.2: (a) The configuration of the proposed transceiver orientation model, (b) The coordinate of the proposed transceiver orientation model

To break the symmetry of the transmitters and the receivers in MIMO OWC channels, this thesis proposes the transceiver orientations as illustrated in Figure 3.2. Besides tilting PDs, LEDs can be tilted as well. This helps improve the worse case performance where the receiver is located at the corner of the room. Figure 3.2 (a)

shows the configuration of the proposed transceiver orientation model where  $\vec{u}_T$  and  $\vec{u}_R$  denote the unit orientation vector of the tilted LEDs and PDs, respectively. In particular,  $\vec{u}_R = [\cos(\beta_R) \sin(\theta_R) \sin(\beta_R) \sin(\theta_R) \cos(\theta_R)]$ . Next,  $\vec{v}_T$  is the unit vector from LED to PD and  $\vec{v}_R$  is unit vector from PD to LED. In spherical coordinates,  $\theta_T$  and  $\theta_R$  are the polar angles measured from the z-axis. These define the tilted angles of the LED and PD with  $0^\circ \leq \theta_T + \theta_R \leq \Psi_c$ , where  $\Psi_c$  denotes the FOV of a PD and  $\Psi_c \leq \pi/2$ , measured from the positive z-axis. In addition,  $\beta_T$  and  $\beta_R$  are the azimuthal angles in the xy-plane with  $0^\circ \leq \beta_T, \beta_R \leq 360^\circ$ , as shown in Figure 3.2 (b). In this research, the azimuthal angle values of the four LEDs and the four PDs are set as  $\beta_T = \beta_R = 45^\circ, 135^\circ, 225^\circ, 315^\circ$  measured from the positive x-axis.

The overall of MIMO OWC configuration can be seen from the top view of the room as in Figure 3.3. There are three different indoor MIMO OWC configurations considered in this part, including 4×4, 9×4, and 16×4 with the coordinates of LEDs shown in Figure 3.3(a)-Figure 3.3(c), respectively. Since the room considered in this system model has a square floor plan, the LED arrangement follows a square grid with the same number of rows and columns. Therefore, 4, 9, and 16 LEDs are considered as these numbers correspond to 2, 3, and 4 rows/columns, respectively. In addition, two receiver positions are considered, as shown in Figure 3.4. The first receiver position is at the center of the room, while the second position is set near a corner. Their coordinates can be specified as R1: (2.5,2.5,0.8) and R2: (1,1,0.8), respectively.



$$\mathbf{H}_k = \mathbf{U}_k \mathbf{\Sigma}_k \mathbf{V}_k^H \quad (3.1)$$

where  $\mathbf{U}_k$  and  $\mathbf{V}_k$  are  $M_r \times M_r$  and  $M_t \times M_t$  unitary matrices, and  $\mathbf{\Sigma}_k$  is an  $M_r \times M_t$  diagonal matrix. For MIMO flip-OFDM, there are  $N/2 - 1$  independent QAM symbols in each OFDM symbol, which utilizes both odd- and even-numbered subcarriers carried by each transmit antenna.



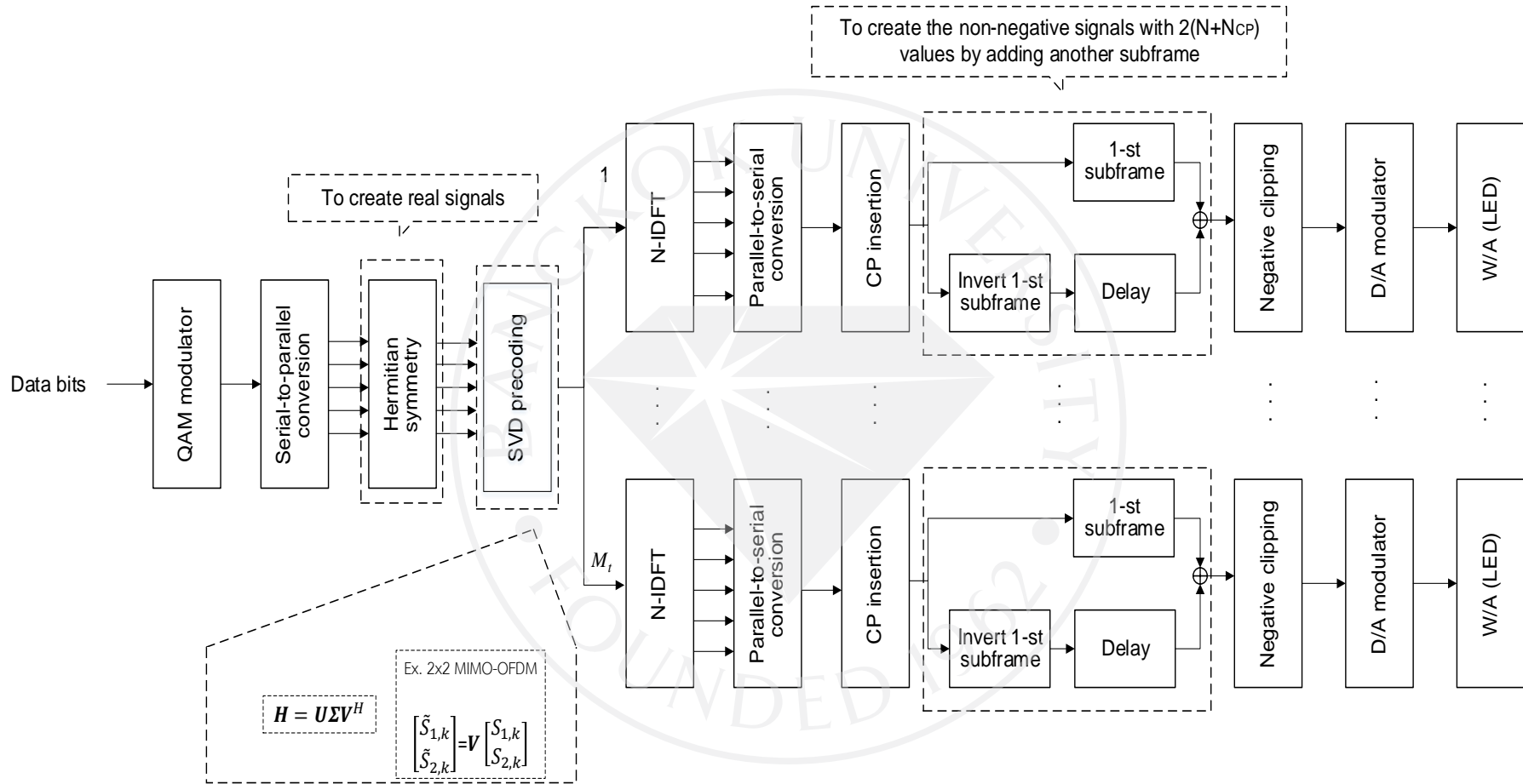


Figure 3.5: The transmission side of the MIMO-flip-OFDM transmission system using SVD



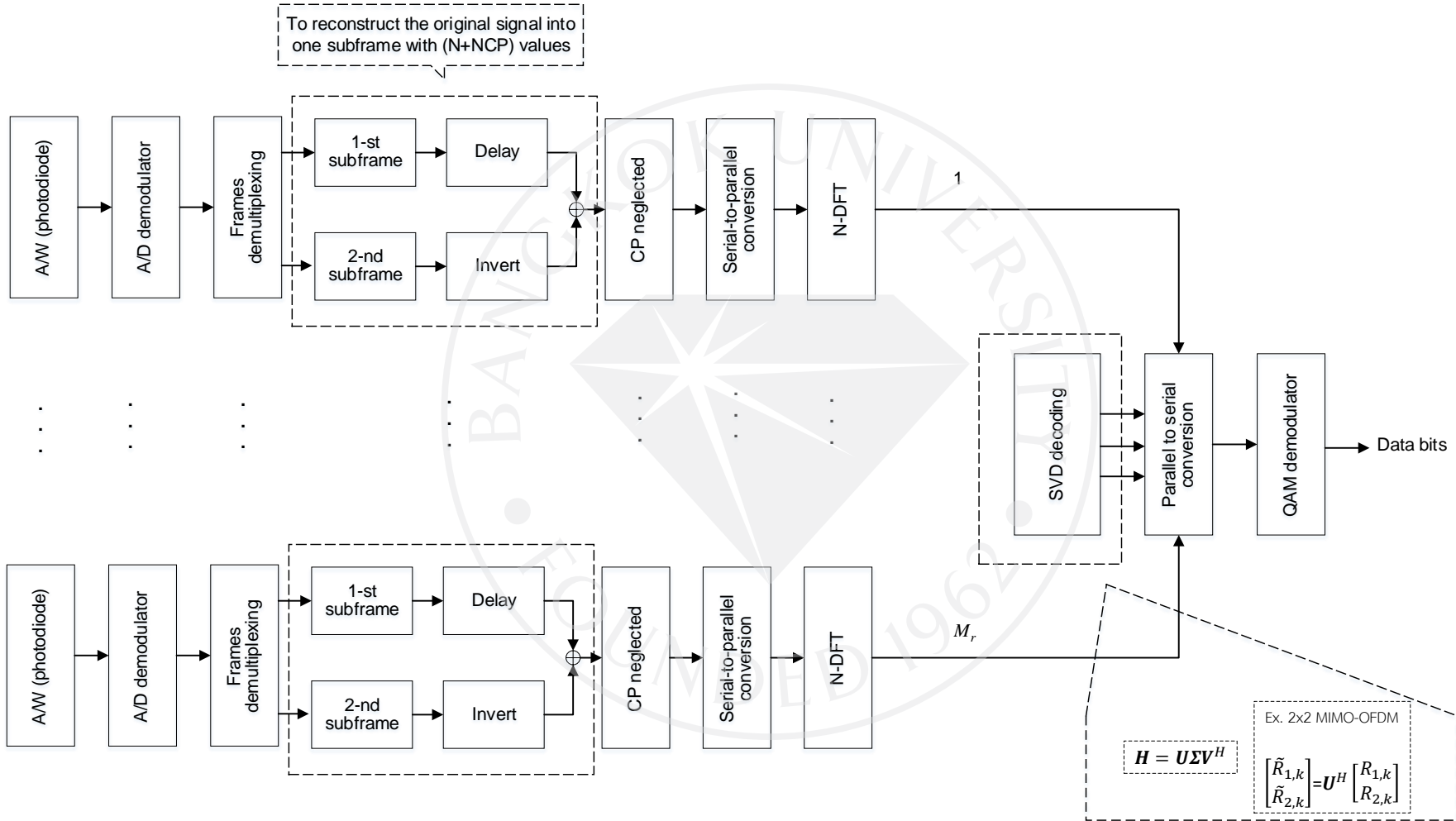


Figure 3.6: The receiving side of the MIMO-flip-OFDM transmission system using SVD

Let  $L_k$  denotes the rank of MIMO channel matrix  $\mathbf{H}_k$  for subcarrier  $k$ , where  $L_k \leq \min\{M_r, M_t\}$ . In what follows, assume that  $M_t = M_r$  and the rank of  $\mathbf{H}$  is equal to  $M_t$ . Denote the QAM symbol on spatial channel  $g$  on subcarrier  $k$  by  $S_{g,k}$  where  $g \in \{1, \dots, L_k\}$  and  $k \in \{0, \dots, N/2 - 1\}$ . Assume that the  $M \times M$ -QAM constellation is employed for each OFDM subcarrier, where  $M \in \{2, 4, 8, 16\}$ . Under Hermitian symmetry, the parallel spatial streams can be shown as

$$\begin{aligned} & 0, S_{1,1}, S_{1,2}, \dots, S_{1,N/2-1}, 0, S_{1,N/2-1}^*, S_{1,N/2-2}^*, \dots, S_{1,1}^* \\ & 0, S_{2,1}, S_{2,2}, \dots, S_{2,N/2-1}, 0, S_{2,N/2-1}^*, S_{2,N/2-2}^*, \dots, S_{2,1}^* \\ & \vdots \\ & 0, S_{M_t,1}, S_{M_t,2}, \dots, S_{M_t,N/2-1}, 0, S_{M_t,N/2-1}^*, S_{M_t,N/2-2}^*, \dots, S_{M_t,1}^* \end{aligned}$$

Suppose that the channel state information (CSI) is known at both transmitter and receiver, by obtaining SVD in Equation (3.1), the transmit QAM symbols on spatial channels are precoded by the unitary matrix  $\mathbf{V}_k$ , yielding

$$\begin{bmatrix} \tilde{S}_{1,k} \\ \tilde{S}_{2,k} \\ \vdots \\ \tilde{S}_{M_t,k} \end{bmatrix} = \mathbf{V}_k \begin{bmatrix} S_{1,k} \\ S_{2,k} \\ \vdots \\ S_{M_t,k} \\ 0 \\ \vdots \\ 0 \end{bmatrix}$$

Next, the transmission process is considered on an individual transmit antenna. Consider LED 1 (transmit antenna 1), the inverse discrete Fourier transform (IDFT) generates  $N$  signal values in the time domain, i.e.,  $\tilde{s}_{1,0}, \tilde{s}_{1,1}, \dots, \tilde{s}_{1,N-1}$ . After serial-to-

parallel (S/P) conversion and cyclic prefix (CP) insertion, the transmit signals can be written as

$$\tilde{s}_{1,N-N_{\text{CP}}}, \dots, \tilde{s}_{1,N-1}, \tilde{s}_{1,0}, \tilde{s}_{1,1}, \dots, \tilde{s}_{1,N-1}$$

To make the signals non-negative, OFDM signals are copied into two consecutive subframes. The 1<sup>st</sup> subframe carries the original OFDM signals while the 2<sup>nd</sup> subframe carries the negative or flipped OFDM signals. Therefore, there are  $2(N + N_{\text{CP}})$  signal values transmitted per flip-OFDM symbol. Let  $\tilde{s}'_{1,n}$  and  $-\tilde{s}'_{1,n}$  denotes the 1<sup>st</sup> subframe (original OFDM signal) and the 2<sup>nd</sup> subframe (negative of the original OFDM signal) of  $\tilde{s}_{1,n}$  carried on LED 1, respectively. Then the combination of two subframes with the CP can be expressed as

$$\tilde{s}'_{1,N-N_{\text{CP}}}, \dots, \tilde{s}'_{1,N-1}, \tilde{s}'_{1,0}, \dots, \tilde{s}'_{1,N-1}, -\tilde{s}'_{1,N-N_{\text{CP}}}, \dots, -\tilde{s}'_{1,N-1}, -\tilde{s}'_{1,0}, \dots, -\tilde{s}'_{1,N-1}$$

From the above expression, the non-negative signals of MIMO flip-OFDM on LED 1 can be obtained by  $\tilde{s}_{1,n}^+ = \max(\tilde{s}_{1,n}, 0)$  and  $\tilde{s}_{1,n}^- = \min(\tilde{s}_{1,n}, 0)$ , resulting in

$$\underbrace{\tilde{s}_{1,N-N_{\text{CP}}}^+, \dots, \tilde{s}_{1,N-1}^+, \tilde{s}_{1,0}^+, \dots, \tilde{s}_{1,N-1}^+}_{\text{CP}}$$

$$-\underbrace{\tilde{s}_{1,N-N_{\text{CP}}}^-, \dots, \tilde{s}_{1,N-1}^-, \tilde{s}_{1,0}^-, \dots, \tilde{s}_{1,N-1}^-}_{\text{CP}}$$

For the purpose of illumination in practice, a DC bias, denoted by  $P_0$ , is added after digital-to-analogue (D/A) modulation and can be adjusted according to the desired dimming level. Since unipolar OFDM signals are considered, there is no restriction on the minimum illumination level to keep the OFDM signals nonnegative. Note that the bias value does not affect transmission performances in the considered

system. Thus, on LED 1, the transmitted optical data signal with pulse period  $T = T_s/2(N + N_{CP})$ , where  $T_s$  is the OFDM symbol period, can be defined as

$$\tilde{s}_1(t) = \alpha_{W/A} P_0 \left[ 1 + m_l \left( \left( \sum_{n=-N_{CP}}^{N-1} (\tilde{s}_{1,n \bmod N}^+) p(t - nT) \right) + \left( \sum_{n=-N_{CP}}^{N-1} (-\tilde{s}_{1,n \bmod N}^-) p(t - nT - (N + N_{CP})T) \right) \right) \right]$$

where  $\alpha_{W/A}$  denotes the optical source conversion factor,  $P_0$  is the DC power,  $m_l$  is the modulation index and  $p(t)$  is the unit-energy rectangular pulse as shown below

$$p(t) = \begin{cases} \frac{1}{\sqrt{T}}, & t \in [0, T) \\ 0, & \text{otherwise} \end{cases}$$

For LED 2, and so on, the transmission process can be repeated as for LED 1, starting from the IDFT step.

Consider LED light with the Lambertian radiation pattern, the channel gain between an LED and a PD of MIMO OWC link is given by (Wu et al., 2016)

$$h_{ij} = \begin{cases} \frac{(m+1)A}{2\pi d_{ij}^2} \cos^m(\phi_T) \cos(\phi_R), & 0 \leq \phi_R \leq \Psi_c \\ 0, & \phi_R \geq \Psi_c \end{cases} \quad (3.2)$$

where  $h_{ij}$  is the gain from LED  $j$  (transmit antenna  $j$ ) to PD  $i$  receive antenna  $i$ ,

$A$  is the receiver collection area,

$m$  is the Lambertian order,

$d_{ij}$  is the distance between LED  $j$  and PD  $i$ ,

$\Psi_c$  is the FOV of the PD where  $\Psi_c \leq \pi/2$ ,

$\phi_T$  is the emission angle at LED  $j$ ,

$\varphi_R$  is the incident angle at PD  $i$ .

At the receiver, the reverse process of the transmitter side is performed.

Assume that  $P_0$  is known at the receiver. Also, the source conversion factor is assumed to be unity for simplicity and without loss of generality; it can be varied by changing the number and/or the type of LEDs used in the transmitter. After removing the DC components, the received signal at time index  $n$  at PD  $i$ , where  $n \in \{0, 1, \dots, N-1\}$  and  $i \in \{1, \dots, M_r\}$ , can be shown as

$$\begin{bmatrix} \tilde{r}_{1,n} \\ \vdots \\ \tilde{r}_{M_r,n} \end{bmatrix} = \alpha_{A/W} m_l \begin{bmatrix} h_{11} & \dots & h_{1M_t} \\ \vdots & \ddots & \vdots \\ h_{M_r1} & \dots & h_{M_rM_t} \end{bmatrix} \begin{bmatrix} \tilde{s}_{1,n} \\ \vdots \\ \tilde{s}_{M_t,n} \end{bmatrix} + \begin{bmatrix} \tilde{n}_{1,n} \\ \vdots \\ \tilde{n}_{M_r,n} \end{bmatrix}$$

where  $\alpha_{A/W}$  is the receiver responsivity (in A/W) and  $\tilde{n}_{i,n}$  is the additive white Gaussian noise (AWGN) with mean 0 and power spectral density (PSD) equal to  $N_0$ . In addition, the above equation can be written in the vector form as

$$\tilde{\mathbf{r}}_n = \alpha_{A/W} m_l \mathbf{H} \tilde{\mathbf{s}}_n + \tilde{\mathbf{n}}_n$$

where  $\tilde{\mathbf{r}}_n$  represents the  $M_r$ -dimensional received symbol vector, at time index  $n$   
 $\tilde{\mathbf{s}}_n$  represents the  $M_t$ -dimensional transmitted symbol vector, at time index  $n$   
 $\tilde{\mathbf{n}}_n$  represents the  $M_r$ -dimensional noise vector, at time index  $n$   
 $\mathbf{H}$  is the  $M_r \times M_t$  matrix of channel gain  $h_{ij}$  from LED  $j$  to PD  $i$ .

Focusing on PD 1, the received signals after discarding the CP are denoted by  $\tilde{r}_{1,0}, \tilde{r}_{1,1}, \dots, \tilde{r}_{1,N-1}$ . Let  $\tilde{R}_{1,0}, \tilde{R}_{1,1}, \dots, \tilde{R}_{1,N-1}$  denote the discrete Fourier transform (DFT) values of  $\tilde{r}_{1,0}, \tilde{r}_{1,1}, \dots, \tilde{r}_{1,N-1}$ , and likewise for other PDs. Then, the DFT value at PD  $i$  on subcarrier  $k$  can be expressed as follows.

$$\tilde{R}_{i,k} = \alpha_{A/W} m_l \sum_{j=1}^{M_t} H_{ij,k} \tilde{S}_{j,k} + \tilde{n}_{i,k} \quad (3.3)$$

In (3.3),  $H_{ij,k}$  is the channel gain from LED  $j$  to PD  $i$  on the subcarrier  $k$  and can be calculated using (3.2), i.e.,  $H_{ij,k} = h_{ij}$  under the line-of-sight assumption,  $\tilde{S}_{j,k}$  denotes the transmitted signal on subcarrier  $k$  at LED  $j$ , and  $\tilde{n}_{i,k}$  denotes the noise on subcarrier  $k$  at PD  $i$ . In addition, noise can be modelled as white Gaussian with mean 0 and variance  $N_0$ , where  $N_0$  denotes the sum of PSD of shot noise and thermal noise (in  $A^2/Hz$ ), i.e.,  $N_0 = N_{0,shot} + N_{0,thermal}$ . Next, the output signals on subcarrier  $k$  from all PDs are decoded by SVD decoding with unitary matrix  $\mathbf{U}_k^H$ , yielding

$$\begin{bmatrix} R_{1,k} \\ R_{2,k} \\ \vdots \\ R_{M_r,k} \end{bmatrix} = \mathbf{U}_k^H \begin{bmatrix} \tilde{R}_{1,k} \\ \tilde{R}_{2,k} \\ \vdots \\ \tilde{R}_{M_r,k} \end{bmatrix}$$

Finally, multiple data streams of the SVD decoder are then extracted into independent parallel spatial channels with different channel gains, denoted by  $\sigma_{1,k}, \dots, \sigma_{L_k,k}$ , from the diagonal entries of  $\mathbf{\Sigma}_k$ . After one-tap equalisation, the received symbol of MIMO flip-OFDM is

$$R'_{g,k} = S_{g,k} + \frac{n_{g,k}}{\alpha_{A/W} m_l \sigma_{g,k}} \quad (3.4)$$

where  $g \in \{1, \dots, L_k\}$  and  $k \in \{0, \dots, N/2 - 1\}$ , and  $n_{g,k}$  results from SVD decoding and DFT of  $\tilde{n}_{i,k}$ . The corresponding data bits can be retrieved using QAM demapping.

### 3.1.3 Bit Loading Technique

The conventional bit loading according to water filling based on the signal's electrical power is used in this research (Panta et al., 2016). Bit loading is processed at the transmitter side where the channel gains, i.e.,  $\sigma_{1,k}, \dots, \sigma_{L,k}$ , are assumed known. Let  $b_{g,k}$  be the number of bits loaded on subcarrier  $k$  on spatial channel  $g$ , where  $b_{g,k} = 2 \log_2 M_{g,k}$ . Accordingly,  $M_{g,k} \times M_{g,k}$ -QAM is applied on subcarrier  $k$  on spatial channel  $g$ . For convenience, 2 bits are loaded in each step in the bit loading algorithm so that square QAM constellations, i.e.,  $2 \times 2$ -,  $4 \times 4$ -,  $8 \times 8$ -, and  $16 \times 16$ -QAM, are used on active subcarriers and spatial channels. Bit loading based on water filling is as follows.

First, calculate the normalized noise level for each subcarrier  $k$  and for each spatial channel  $g$  by dividing the noise power by channel gain as  $N_{0,g,k} = N_0 / \sigma_{g,k}^2$ . Second, set the initial water level  $n_{g,k} = N_{0,g,k}$  and search for the lowest water level. Next, assign 2 bits to the subcarrier and the spatial channel with the lowest water level, and then update the number of bits loaded as  $b_{g,k} = b_{g,k} + 2$ . Then, calculate the signal energy  $E_{s,g,k}$  on this subcarrier and spatial channel based on the BER target for uncoded transmission at  $10^{-5}$ , and update the new water level to  $n_{g,k} = N_{0,g,k} + E_{s,g,k}$ . Finally, repeat the process until the total number of allocated bits is equal to the target number of bits per OFDM symbol.

### 3.1.4 Transmit Optical Power Analysis for MIMO Flip-OFDM

To compute the mean transmit optical power for MIMO flip-OFDM using SVD. First, consider the transmit QAM symbols on spatial channels which are precoded by the unitary matrix  $\mathbf{V}_k$  as

$$\begin{bmatrix} \tilde{S}_{1,k} \\ \tilde{S}_{2,k} \\ \vdots \\ \tilde{S}_{M_t,k} \end{bmatrix} = \mathbf{V}_k \begin{bmatrix} S_{1,k} \\ S_{2,k} \\ \vdots \\ S_{M_t,k} \\ 0 \\ \vdots \\ 0 \end{bmatrix} \quad (3.5)$$

where

$$\mathbf{V}_k = \begin{bmatrix} v_{11,k} & \dots & v_{1M_t,k} \\ \vdots & \ddots & \vdots \\ v_{M_t1,k} & \dots & v_{M_tM_t,k} \end{bmatrix}$$

The precoded transmit QAM symbols can be written in terms of linear combination of the QAM symbols from all spatial channels. For example, the transmit data carried on LED 1 is

$$\tilde{S}_{1,k} = v_{11,k}S_{1,k} + v_{12,k}S_{2,k} + \dots + v_{1M_t,k}S_{M_t,k}$$

After that, by IDFT definition, the transmit signal in the time domain for MIMO-flip-OFDM using SVD on LED 1 can be rewritten as

$$\tilde{s}_{1,n} = \frac{1}{\sqrt{N}} \sum_{k=0}^{N-1} \tilde{S}_{1,k} e^{i2\pi kn/N}, n \in \{0, \dots, N-1\}$$

According to (Dissanayake and Armstrong, 2013), the mean transmit optical power of flip-OFDM is  $P = E\{\tilde{s}_1(t)\} = \frac{m_1 \sigma_{\tilde{s}_{1,n}}}{\sqrt{2\pi T}}$ . To use the expression, the standard



deviation of  $\tilde{s}_{1,n}$ , i.e.,  $\sigma_{\tilde{s}_{1,n}}$  can be computed based on the Hermitian symmetry condition together with  $S_0 = S_{N/2} = 0$  as follows.

$$\tilde{s}_{1,n} = \frac{1}{\sqrt{N}} \left\{ \sum_{k=1}^{N/2-1} \tilde{S}_{1,k} e^{i2\pi kn/N} + \sum_{k=N/2+1}^{N-1} \tilde{S}_{1,k} e^{i2\pi kn/N} \right\}$$

Then, apply  $S_{N-k} = S_k^*$ ,  $k = \{1, \dots, N/2 - 1\}$ , by changing  $k$  to  $N - k'$  at the second term, yielding

$$\begin{aligned} \tilde{s}_{1,n} &= \frac{1}{\sqrt{N}} \left\{ \sum_{k=1}^{N/2-1} \tilde{S}_{1,k} e^{i2\pi kn/N} + \sum_{k'=1}^{N/2-1} \tilde{S}_{N-k'} e^{i2\pi(N-k')n/N} \right\} \\ &= \frac{1}{\sqrt{N}} \left\{ \sum_{k=1}^{N/2-1} \tilde{S}_{1,k} e^{i2\pi kn/N} + \sum_{k'=1}^{N/2-1} \tilde{S}_{1,k'}^* e^{-i2\pi k'n/N} \right\} \\ &= \frac{1}{\sqrt{N}} \left\{ \sum_{k=1}^{N/2-1} (\tilde{S}_{1,k} e^{i2\pi kn/N} + \tilde{S}_{1,k}^* e^{-i2\pi kn/N}) \right\} \\ &= \frac{2}{\sqrt{N}} \sum_{k=1}^{N/2-1} \left( \Re\{\tilde{S}_{1,k}\} \cos\left(\frac{2\pi kn}{N}\right) - \Im\{\tilde{S}_{1,k}\} \sin\left(\frac{2\pi kn}{N}\right) \right) \end{aligned}$$

So, the variance of  $\tilde{s}_{1,n}$  is

$$\begin{aligned} \text{var}[\tilde{s}_{1,n}] &= \frac{4}{N} \sum_{k=1}^{N/2-1} \left( \cos^2\left(\frac{2\pi kn}{N}\right) \text{var}[\Re\{\tilde{S}_{1,k}\}] \right. \\ &\quad \left. + \sin^2\left(\frac{2\pi kn}{N}\right) \text{var}[\Im\{\tilde{S}_{1,k}\}] \right) \end{aligned} \quad (3.6)$$

For large  $N$ , the distribution of  $\tilde{s}_{1,n}$  approaches the Gaussian distribution. In addition, the employed  $M \times M$ -QAM constellations have IID real and imaginary parts with zero mean and the same variance where  $\text{var}[\Re\{S_{1,k}\}]$  is equal to  $\text{var}[\Im\{S_{1,k}\}]$ , yielding

$$\text{var}[\Re\{\tilde{S}_{1,k}\}] = \text{var}[\Im\{\tilde{S}_{1,k}\}] = \frac{E[|\tilde{S}_{1,k}|^2]}{2}$$

Thus,

$$\begin{aligned} \text{var}[\tilde{s}_{1,n}] &= \frac{4}{N} \sum_{k=1}^{N/2-1} \text{var}[\Re\{\tilde{S}_{1,k}\}] \\ &= \frac{2}{N} \sum_{k=1}^{N/2-1} E[|\tilde{S}_{1,k}|^2] \end{aligned}$$

According to  $\tilde{S}_{1,k} = v_{11,k}S_{1,k} + v_{12,k}S_{2,k} + \dots + v_{1L_k,k}S_{L_k,k}$ , it follows that

$$E[|\tilde{S}_{1,k}|^2] = \sum_{g=1}^{N/2-1} \sum_{g=1}^{L_k} |v_{1g,k}|^2 E[|S_{j,k}|^2]$$

Therefore, the variance of  $\tilde{s}_{1,n}$  can be shown as

$$\text{var}[\tilde{s}_{1,n}] = \frac{2}{N} \sum_{k=1}^{N/2-1} \sum_{g=1}^{L_k} |v_{1g,k}|^2 E[|S_{j,k}|^2]$$

Finally, the mean transmit optical power of flip-OFDM at transmit antenna 1 is

$$\begin{aligned} P_{tx1} &= E\{\tilde{s}_1(t)\} = \frac{m_l \sigma_{\tilde{s}_{1,n}}}{\sqrt{2\pi T}} \\ &= \frac{m_l}{\sqrt{2\pi T}} \sqrt{\frac{2}{N} \sum_{k=1}^{N/2-1} \sum_{g=1}^{L_k} |v_{1g,k}|^2 E[|S_{j,k}|^2]} \\ &= m_l \sqrt{\frac{1}{\pi N T} \sum_{k=1}^{N/2-1} \sum_{g=1}^{L_k} |v_{1g,k}|^2 E[|S_{j,k}|^2]} \end{aligned}$$

For LED 2, and so on, the mean transmit optical power can be calculated in the same way as for LED 1. The total transmit optical power of all transmit LEDs can be written as

$$P_T^{\text{total}} = P_{tx1} + \dots + P_{txM_t}$$

From above equation, the total transmit optical power in terms of the minimum distance  $d$  is

$$P_T^{\text{total}} = \frac{m_l d}{\sqrt{6\pi NT}} \left( \sum_{j=1}^{M_t} \sqrt{\sum_{k=1}^{N/2-1} \sum_{g=1}^{L_k} |v_{jg,k}|^2 (M_{g,k}^2 - 1)} \right) \quad (3.7)$$

### 3.1.5 BER Performance Analysis with Bit Loading

In order to compute the BER of MIMO flip- OFDM using SVD with bit loading, the BER expression can be taken from the union bound estimate on  $M \times M$ -QAM as in (Proakis and Salehi, 2008). For bit loading,  $b_{g,k}$  is defined as the number of bits loaded on subcarrier  $k$  on spatial channel  $g$ , where  $b_{g,k} = 2 \log_2 M_{g,k}$ . In addition,  $M_{g,k} \times M_{g,k}$ -QAM is applied on subcarrier  $k$  on spatial channel  $g$  and the weighted factor for bits allocated to subcarrier  $k$  and spatial channel  $g$  is  $b_{g,k} / b_{\text{OFDM}}$ , where  $b_{\text{OFDM}}$  is the total number of bits transmitted on all spatial channels and subcarriers per OFDM symbol. The resultant BER expression is

$$\text{BER} \approx \sum_{k=1}^{N/2-1} \sum_{g=1}^{L_k} \frac{b_{g,k}}{b_{\text{OFDM}}} \times \frac{2(M_{g,k} - 1)}{M_{g,k} \log_2 M_{g,k}} Q \left( \sqrt{\frac{6 \log_2 M_{g,k} E_{b,g,k}}{(M_{g,k}^2 - 1) N_{0,g,k}}} \right) \quad (3.8)$$

where  $E_{b,g,k}$  and  $N_{0,g,k}$  are the energy per bit and the noise variance on subcarrier  $k$  on spatial channel  $g$  at the receiver respectively.

The received signal of MIMO flip-OFDM can be written as

$$R_{g,k} = \alpha_{A/W} m_l \sigma_{g,k} S_{j,k} + n_{g,k} \quad (3.9)$$

where  $g \in \{1, \dots, L_k\}$  is spatial channel index and  $k \in \{1, \dots, N/2 - 1\}$  is subcarrier index. From Equation (3.9), by shaping the received signal with the singular value  $\sigma_{j,k}$ ,

$$R_{g,k} = S_{g,k} + \frac{n_{g,k}}{\alpha_{A/W} m_l \sigma_{g,k}} \quad (3.10)$$

From above equation,  $E_{b,g,k}$  and  $N_{0,g,k}$  can be expressed as (3.11) and (3.12), respectively.

$$E_{b,g,k} = \frac{E_{s,g,k}}{2 \log_2 M_{g,k}} = \frac{d^2 (M_{g,k}^2 - 1)}{12 \log_2 M_{g,k}} \quad (3.11)$$

In Equation (3.11),  $E_{s,g,k} = d^2 (M_{g,k}^2 - 1)/6$  and  $d$  is the minimum distance between signal points. In addition,  $N_{0,g,k}$  can be compute as

$$N_{0,g,k} = \frac{N_0}{\alpha_{A/W}^2 m_l^2 \sigma_{g,k}^2} \quad (3.12)$$

where the variance of noise for flip-OFDM is  $N_0$ . Substituting (3.11) and (3.12) into (3.8), it follows that

$$\text{BER} \approx \sum_{k=1}^{N/2-1} \sum_{g=1}^{L_k} \frac{b_{g,k}}{b_{\text{OFDM}}} \times \frac{2(M_{g,k} - 1)}{M_{g,k} \log_2 M_{g,k}} Q \left( \sqrt{\frac{d^2 \alpha_{A/W}^2 m_l^2 \sigma_{g,k}^2}{2N_0}} \right) \quad (3.13)$$

According to (3.7), the minimum distance with respect to the transmit optical power is given as

$$d = \frac{P_T^{\text{total}} \sqrt{6\pi NT}}{m_l \sum_{j=1}^{M_t} \sqrt{\sum_{k=1}^{N/2-1} \sum_{g=1}^{L_k} |v_{jg,k}|^2 (M_{g,k}^2 - 1)}} \quad (3.14)$$

The pulse period  $T$  can be calculated in terms of the data rate from the relationship

$$R = \frac{b_{\text{OFDM}}}{T_{\text{OFDM}}} = \frac{b_{\text{OFDM}}}{2NT} \quad (3.15)$$

From (3.15), substituting  $T$  into (3.14),

$$d = \frac{P_T^{\text{total}}}{m_l} \sqrt{\frac{3\pi b_{\text{OFDM}}}{R}} \frac{1}{\sum_{j=1}^{M_t} \sqrt{\sum_{k=1}^{N/2-1} \sum_{g=1}^{L_k} |v_{jg,k}|^2 (M_{g,k}^2 - 1)}} \quad (3.16)$$

Finally, to obtain the BER expression for MIMO flip-OFDM using SVD with bit loading, substituting  $d$  from (3.16) to (3.13), resulting in

$$\text{BER} \approx \frac{4}{b_{\text{OFDM}}} \sum_{k=1}^{N/2-1} \sum_{g=1}^{L_k} \frac{(M_{g,k} - 1)}{M_{g,k}} \times Q \left( \sqrt{\frac{3\pi b_{\text{OFDM}}}{2N_0 R}} \times \frac{\alpha_{A/W} \sigma_{g,k} P_T^{\text{total}}}{\sum_{j=1}^{M_t} \sqrt{\sum_{k=1}^{N/2-1} \sum_{g=1}^{L_k} |v_{jg,k}|^2 (M_{g,k}^2 - 1)}} \right) \quad (3.17)$$

### 3.2 MU-MIMO for an Indoor OWC System

In this section, system models including of the system configuration, the transmitted and received signals, BD precoding and combining, user throughputs, and user grouping methods are presented.

#### 3.2.1 System Configurations of MU-MIMO

Figure 3.7 shows the configuration of the indoor MU-MIMO OWC system for downlink data transmissions. Assume a room with the dimension of  $5 \text{ m} \times 5 \text{ m} \times 2.5 \text{ m}$ .

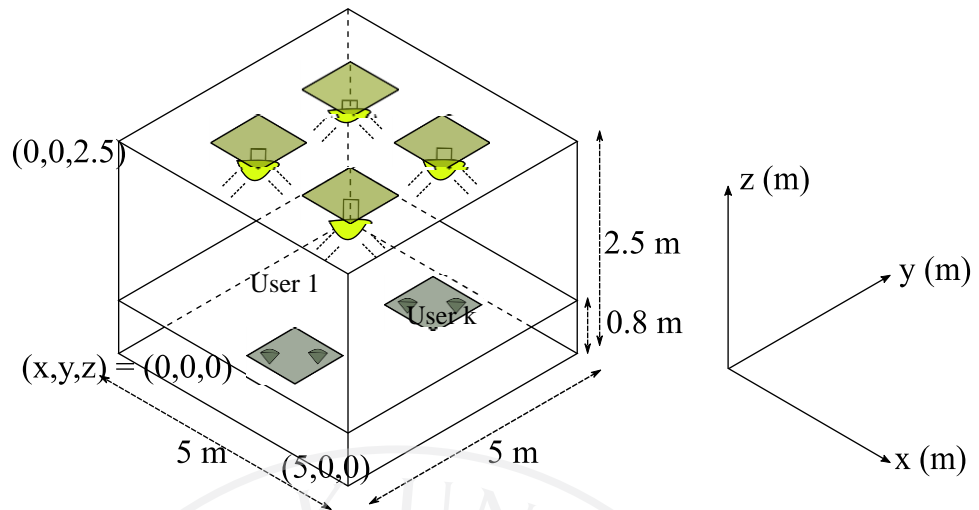


Figure 3.7: Room dimension and coordinates (in m) of the indoor MU-MIMO OWC system.

The system consists of  $M_t$  LEDs, which are positioned at the height of 2.5 m above the floor. There are  $K$  users each with  $M_r'$  PDs placed at the height of 0.8 m from the floor. The total number of PDs from all users is  $M_r = KM_r'$ . Assume that  $M_r > M_t$ . For simplicity, this research assumes that  $M_r/M_t$  and  $M_t/M_r'$  are positive integers. Accordingly, there will be  $G = M_r/M_t$  groups each containing  $K' = M_t/M_r'$  users. When this integer assumption does not hold, user group sizes may vary and user grouping method can be investigated through the adjustment of group sizes.

### 3.2.2 Transmitted and Received Signals

In Figure 3.8, a MU-MIMO OWC with IM/DD and time division multiplexing (TDM) is illustrated for a group of  $K'$  users. Let  $\mathbf{x}_k$  be the  $M_r' \times 1$  vector of data symbols intended for user  $k$  where  $k \in \{1, \dots, K'\}$ . Assuming that  $\mathbf{x}_k$  is based on pulse amplitude modulation (PAM), has zero mean and is normalized to the range of  $[-1, 1]$ , so

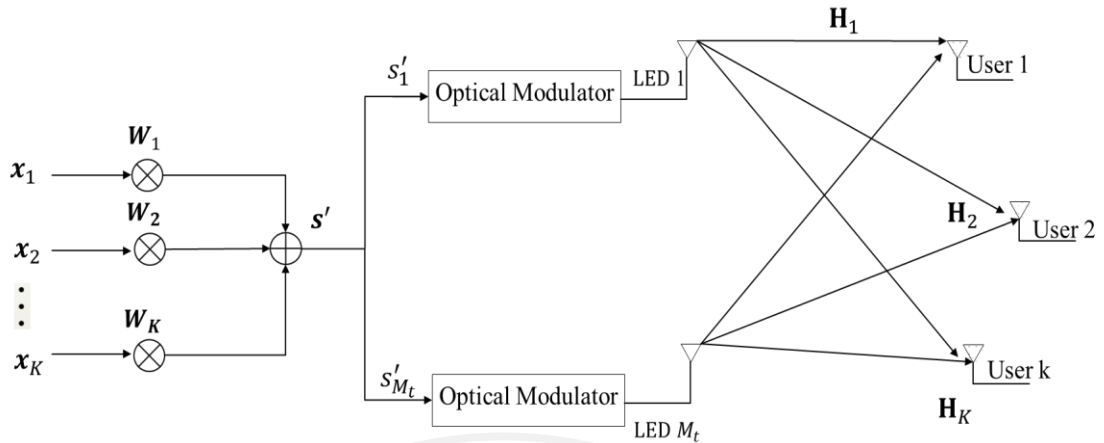


Figure 3.8: Schematic diagram of indoor MU-MIMO OWC

the average of  $\mathbf{x}_k$  is zero vector. For user  $k$ ,  $\mathbf{x}_k$  is multiplied by a precoding matrix  $\mathbf{W}_k$ . Therefore, for all users, the precoded data signal vector for  $M_t$  transmit LEDs is given by

$$\mathbf{s}' = \sum_{k=1}^{K'} \mathbf{W}_k \mathbf{x}_k \quad (3.18)$$

Due to IM/DD propagation,  $\mathbf{s}'$  must contain non-negative signal values. To produce non-negative input signal to LED, a bias is added to the transmitted signal. Thus, the transmitted signals from LED transmitters can be expressed as

$$\mathbf{s} = P \left( \mathbf{1} + m_l \sum_{k=1}^{K'} \mathbf{W}_k \mathbf{x}_k \right) \quad (3.19)$$

where  $P$  is the average signal value at each LED transmitter, the vector  $\mathbf{1}$  corresponds to the bias, and  $m_l$  is the modulation index ( $0 < m_l \leq 1$ ) which ensures that the LED operates in its linear region and avoids over-modulation induced clipping.

Consider the multiuser MIMO link between the LED array and user  $k$ . In general, there are two main types of signal propagation in OWC systems, which are

the LOS and non-LOS components. While non-LOS components of light propagation also exist, e.g., due to reflections, LOS components dominate for most indoor usage scenarios. Therefore, only LOS components are considered. In (3.20), the MIMO channel matrix of user  $k$ , i.e.,  $\mathbf{H}_k$ , contains the values of path losses, where  $h_{k,ij}$  denotes the path loss from LED transmitter  $j$  to PD  $i$  for user  $k$ .

$$\mathbf{H}_k = \begin{bmatrix} h_{k,11} & \dots & h_{k,1M_t} \\ \vdots & \ddots & \vdots \\ h_{k,M_r1} & \dots & h_{k,M_rM_t} \end{bmatrix} \quad (3.20)$$

For OWC systems,  $h_{k,ij}$  can be computed using the LOS channel model expresses as

$$h_{k,ij} = \begin{cases} \frac{(m+1)A}{2\pi d_{k,ij}^2} \cos^m(\phi_{k,ij}) \cos(\varphi_{k,ij}), & 0 \leq \varphi_{k,ij} \leq \Psi_{\text{FOV}} \\ 0, & \varphi_{k,ij} \geq \Psi_{\text{FOV}} \end{cases} \quad (3.21)$$

where  $d_{k,ij}$  is the distance from LED  $j$  to PD  $i$  for user  $k$ ,  $\phi_{k,ij}$  is the emission angle from LED  $j$  to PD  $i$  for user  $k$ ,  $\varphi_{k,ij}$  is the incidence angle from LED  $j$  to PD  $i$  for user  $k$ ,  $A$  is the PD detection surface area,  $\Psi_{\text{FOV}}$  is the FOV of each PD, and  $m$  is the order of Lambertian radiation related to the LED semiangle at half the maximum power  $\Phi_{1/2}$  by  $m = -\log(2)/\log(\cos \Phi_{1/2})$ .

Note that the shadowing can occur due to random movements of people and objects, and can cause outages of data transmission. This work considers optimization of user grouping based on long-term channel conditions. Therefore, intermittent outages of data transmission due to shadowing are not considered.

At the receiver, the received optical signal at the  $k$ -th user can be written as



$$\mathbf{r}'_k = \alpha_{A/W} \mathbf{H}_k \begin{bmatrix} s_1 \\ s_2 \\ \vdots \\ s_{M_t} \end{bmatrix} + \mathbf{n}_k = \alpha_{A/W} \mathbf{H}_k P \begin{bmatrix} 1 + m_l s'_1 \\ 1 + m_l s'_1 \\ \vdots \\ 1 + m_l s'_{M_t} \end{bmatrix} + \mathbf{n}_k \quad (3.22)$$

After removing the DC components, the received signal can be written as

$$\mathbf{r}_k = \alpha_{A/W} m_l P \mathbf{H}_k \begin{bmatrix} s'_1 \\ s'_1 \\ \vdots \\ s'_{M_t} \end{bmatrix} + \mathbf{n}_k \quad (3.23)$$

where  $\mathbf{r}_k$  is  $M'_r \times 1$  vector containing received signal values at the  $M'_r$  PDs for user  $k$ ,  $\alpha_{A/W}$  is the receiver responsivity,  $\mathbf{H}_k$  is a  $M'_r \times M_t$  MIMO channel matrix for user  $k$ , and  $\mathbf{n}_k$  is a  $M'_r \times 1$  noise vector for user  $k$  that contain IID Gaussian random variables with mean 0 and variance  $\sigma_{AWGN}^2$ .

From (3.19), after the DC bias is removed, the expression in (3.23) can be written as

$$\begin{aligned} \mathbf{r}_k &= \alpha_{A/W} m_l P \mathbf{H}_k \sum_{i=1}^{K'} \mathbf{W}_i \mathbf{x}_i + \mathbf{n}_k \\ &= \alpha_{A/W} m_l P [\mathbf{H}_k \mathbf{W}_k \mathbf{x}_k + \mathbf{H}_k \sum_{i=1, i \neq k}^{K'} \mathbf{W}_i \mathbf{x}_i] + \mathbf{n}_k \end{aligned} \quad (3.24)$$

where  $\mathbf{H}_k \mathbf{W}_k \mathbf{x}_k$  is the desired received signal while  $\mathbf{H}_k \sum_{i=1, i \neq k}^{K'} \mathbf{W}_i \mathbf{x}_i$  is the MUI term.

### 3.2.3 BD Precoding and Combining

In order to eliminate the interference term, the BD technique is applied within each group of  $K'$  users. Consider an arbitrary group of users indexed by  $1, \dots, K'$ . For user  $k \in \{1, \dots, K'\}$ , the precoding matrix  $\mathbf{W}_k$  is computed using the following steps.

Step 1: Form the  $(K' - 1)M'_r \times M_t$  matrix

$$\tilde{\mathbf{H}}_k = \begin{bmatrix} \mathbf{H}_1 \\ \vdots \\ \mathbf{H}_{k-1} \\ \mathbf{H}_{k+1} \\ \vdots \\ \mathbf{H}_{k'} \end{bmatrix}. \quad (3.25)$$

Step 2: Use SVD to write

$$\tilde{\mathbf{H}}_k = \tilde{\mathbf{U}}_k \tilde{\mathbf{\Sigma}}_k \tilde{\mathbf{V}}_k. \quad (3.26)$$

Step 3: Write

$$\tilde{\mathbf{V}}_k = [\tilde{\mathbf{V}}_k^1 \quad \tilde{\mathbf{V}}_k^0], \quad (3.27)$$

where  $\tilde{\mathbf{V}}_k^0$  contains the last  $M'_r$  columns of  $\tilde{\mathbf{V}}_k$  and is the basis matrix for the null space of  $\tilde{\mathbf{H}}_k$ . Note that  $\tilde{\mathbf{V}}_k^0$  is  $M_t \times M'_r$ .

Step 4: Form the  $M'_r \times M'_r$  matrix

$$\bar{\mathbf{H}}_k = \mathbf{H}_k \tilde{\mathbf{V}}_k^0. \quad (3.28)$$

Step 5: Use SVD to write

$$\bar{\mathbf{H}}_k = \bar{\mathbf{U}}_k \bar{\mathbf{\Sigma}}_k \bar{\mathbf{V}}_k^H. \quad (3.29)$$

Step 6: Form the  $M_t \times M'_r$  precoding matrix

$$\mathbf{W}_k = \tilde{\mathbf{V}}_k^0 \bar{\mathbf{V}}_k. \quad (3.30)$$

From (3.30) and the fact that  $\tilde{\mathbf{V}}_k^0$  is the basis for the null space of  $\tilde{\mathbf{H}}_k$ , which contains the MIMO channel matrices of all users except for user  $k$ , it follows that the signals transmitted to user  $k$  will not be received by any other user. Therefore, BD precoding can prevent MUI.

On the receiver side, user  $k$  performs signal combining using the  $M'_r \times M'_r$  matrix  $\tilde{\mathbf{U}}_k^H$ . Over all, BD precoding and combining yield  $M'_r$  spatial channels for user

$k$  with the effective path losses  $\sigma_{k,1}, \dots, \sigma_{k,M'_r}$ , which are the diagonal entries of the  $M'_r \times M'_r$  diagonal matrix  $\bar{\Sigma}_k$ .

### 3.2.4 User Throughputs

After signal combining using  $\tilde{\mathbf{U}}_k^H$  and removing the signal averages which do not contain any information, the combined signals can be expressed as

$$\mathbf{v}_k = \tilde{\mathbf{U}}_k^H \mathbf{r}_k = \alpha_{A/W} m_l P \bar{\Sigma}_k \mathbf{x}_k + \mathbf{n}'_k \quad (3.31)$$

where the noise vector  $\mathbf{n}'_k = \tilde{\mathbf{U}}_k^H \mathbf{n}_k$  has the same statistics as the noise vector  $\mathbf{n}_k$  before signal combining. i.e., containing IID Gaussian random variables with mean 0 and variance  $\sigma_{\text{AWGN}}^2$ .

Let  $E_s$  denotes the mean square of data symbols, i.e., average symbol energy. Using the Shannon's capacity formula, the average total throughput of user  $k$  (in bit/s/Hz) over  $M'_r$  spatial channels with  $G$  TDM time slots (for  $G$  user groups) is

$$\begin{aligned} C_k &= \frac{1}{G} \sum_{n=1}^{M'_r} \log_2 \left( 1 + \frac{\alpha_{A/W}^2 P^2 m_l^2 \sigma_{k,n}^2 E_s}{\sigma_{\text{AWGN}}^2} \right) \\ &= \frac{1}{G} \sum_{n=1}^{M'_r} \log_2 (1 + K_{\text{SNR}} \sigma_{k,n}^2), \end{aligned} \quad (3.32)$$

where

$$K_{\text{SNR}} = \frac{\alpha_{A/W}^2 P^2 m_l^2 E_s}{\sigma_{\text{AWGN}}^2} \quad (3.33)$$

In a multiuser scenario, user throughputs can differ depending on their path losses. For fairness among users, the minimum throughput among users is considered as the performance measure.

### 3.2.5 Heuristics for User Grouping

The user throughput in (3.32) depends on the user grouping in a complicated fashion. In particular, the SNRs ( $K_{\text{SNR}}\sigma_{k,n}^2$ ) in (3.32) depend on the path losses ( $\sigma_{k,n}^2$ ) that are obtained after the computation of BD precoding. As the result, while an optimization problem of user grouping can be formulated, the optimization problem is general a nonlinear problem that is numerically difficult to solve. Therefore, in what follows, heuristics for user grouping are proposed, with their performances evaluated.

Intuitively, user grouping should be done to avoid “highly correlated” channel matrices among users in the same group, where different correlation measures are used in different heuristics below. This is because BD precoding relies on projecting the user's MIMO channel matrix onto the null space of the other users' MIMO channel matrices in the same group. Three different heuristics to prevent high pairwise channel correlations among users in the same group are proposed as follows.

Method 1: Group the users to maximize the average distance between users in the same group, where the distance between users  $k$  and  $l$  is defined as

$$D_{kl} = \|\mathbf{u}_k - \mathbf{u}_l\|, \quad (3.34)$$

where  $\mathbf{u}_k$  and  $\mathbf{u}_l$  denote the location vectors of users  $k$  and  $l$ , respectively. Roughly speaking, since users located close to each other tend to have similar MIMO channel matrices, maximizing the average distance within each group should prevent highly correlated channel matrices.

Method 2: Group the users to minimize the average correlation coefficient between users in the same group, where the correlation coefficient is given by

$$R_{kl} = \frac{|\text{tr}(\mathbf{H}_k \mathbf{H}_l^T)|}{\|\mathbf{H}_k\|_F \|\mathbf{H}_l\|_F}, \quad (3.35)$$

Note that  $\text{tr}(\mathbf{A})$  denotes the trace of matrix  $\mathbf{A}$ , which is the sum of diagonal entries of  $\mathbf{A}$ .  $\|\mathbf{B}\|_F$  denotes the Frobenius norm of matrix  $\mathbf{B}$ , which is square root of the sum of all entries squared. For example, if

$$\mathbf{A} = \begin{bmatrix} a_{11} & a_{12} \\ a_{21} & a_{22} \end{bmatrix}$$

$$\mathbf{B} = \begin{bmatrix} b_{11} & b_{12} & b_{13} \\ b_{21} & b_{22} & b_{23} \end{bmatrix}$$

Then

$$\text{tr}(\mathbf{A}) = a_{11} + a_{22}$$

$$\|\mathbf{B}\|_F = \sqrt{b_{11}^2 + b_{12}^2 + b_{13}^2 + b_{21}^2 + b_{22}^2 + b_{23}^2}$$

The definition of  $R_{kl}$  tries to capture the similarity between channel matrices of users  $k$  and  $l$ . Its value is between 0 and 1 (Czink et al., 2009).

Method 3: Group the users to maximize the average normalized matrix norm of its projection on the other user's nullspace, where the pairwise normalized matrix norm is defined as

$$N_{kl} = \min \left( \frac{\|\mathbf{H}_k \mathbf{V}_l^0\|_F}{\|\mathbf{H}_k\|_F}, \frac{\|\mathbf{H}_l \mathbf{V}_k^0\|_F}{\|\mathbf{H}_l\|_F} \right), \quad (3.36)$$

where  $\mathbf{V}_k^0$  denoted a  $M_t \times (M_t - M_r)$  basis matrix for the nullspace of  $\mathbf{H}_k$ . Note that  $\mathbf{V}_k^0$  contains the last  $(M_t - M_r)$  columns of  $\mathbf{V}_k$  obtained from the SVD  $\mathbf{H}_k = \mathbf{U}_k \mathbf{\Sigma}_k \mathbf{V}_k^H$ .

Method 3 is proposed based on how BD precoding operates. Recall that the user's precoding matrix is chosen to be in the null space of all the other users' channel

matrices. Each fraction in the definition of  $N_{kl}$  captures how much energy survives in the transmitted signals if they are projected onto the null space of the other user's MIMO channel matrix; its value is between 0 and 1.

Finally, a hybrid method is considered, where all three methods are applied and the best user grouping among them is selected as the final answer.

### 3.2.6 ILP Formulation for User Grouping

The three methods of user grouping as proposed in the previous section can be formulated as integer linear programming (ILP) problems that can be practically solved using ILP software, e.g., GNU Linear Programming Kit (GLPK). To avoid repetitions, each method can be formulated as minimizing the maximum average pairwise parameter  $\gamma_{kl}$  between all pairs of users in the same group, where the pairwise parameter is defined below.

$$\gamma_{kl} = \begin{cases} -D_{kl}, & \text{method 1} \\ R_{kl}, & \text{method 2} \\ -N_{kl}, & \text{method 3} \end{cases} \quad (3.37)$$

Note that the values of  $\gamma_{kl}$  for all user pairs can be precomputed using (3.34), (3.35), and (3.36). Then, they can be used as input parameters for solving the optimization problems.

Define two sets of decision variables for optimization. Let  $x_k^g \in \{0,1\}$ , where  $k \in \{1, \dots, K\}$  and  $g \in \{1, \dots, G\}$ , be equal to 1 if user  $k$  is assigned to group  $g$ , and 0 otherwise. Let  $y_{kl}^g \in \{0,1\}$ , where  $k, l \in \{1, \dots, K\}$  and  $g \in \{1, \dots, G\}$ , be equal to 1 if and only if users  $k$  and  $l$  are both assigned to group  $g$ .

Below is an optimization problem for each user grouping method. For notational convenience, let  $\mathcal{K} \in \{1, \dots, K\}$  and  $\mathcal{G} \in \{1, \dots, G\}$ .

$$\min \max_{g \in \mathcal{G}} \frac{1}{K'(K'-1)} \sum_{k,l \in \mathcal{K}, k \neq l} \gamma_{kl} y_{kl}^g \quad (3.38)$$

$$\text{s. t. } \forall k \in \mathcal{K} \quad \sum_{g=1}^G x_k^g = 1 \quad (3.39)$$

$$\forall g \in \mathcal{G} \quad \sum_{k=1}^K x_k^g = K' \quad (3.40)$$

$$\forall k, l \in \mathcal{K}, k \neq l, \forall g \in \mathcal{G} \quad y_{kl}^g \geq x_k^g + x_l^g - 1 \quad (3.41)$$

$$\text{and } y_{kl}^g \leq x_k^g \text{ and } y_{kl}^g \leq x_l^g$$

$$\forall k \in \mathcal{K}, \forall g \in \mathcal{G} \quad x_k^g \in \{0,1\} \quad (3.42)$$

$$\forall k, l \in \mathcal{K}, k \neq l, \forall g \in \mathcal{G} \quad y_{kl}^g \in \{0,1\} \quad (3.43)$$

The objective in (3.38) is to maximize the average pairwise parameter  $\gamma_{kl}$  in each group. The set of constraints in (3.39) ensure that each user is assigned to exactly one group. The set of constraints in (3.40) ensure that exactly  $K'$  users are assigned to each group. The set of constraints in (3.41) ensure that  $y_{kl}^g = 1$  when users  $k$  and  $l$  are assigned to group  $g$ , and  $y_{kl}^g = 0$  otherwise.

By introducing one additional decision variable  $z$  to take the value of

$$\max_{g \in \mathcal{G}} \frac{1}{K'(K'-1)} \sum_{k,l \in \mathcal{K}, k \neq l} \gamma_{kl} y_{kl}^g,$$

the above optimization problem can be written as an ILP problem shown below. Note that the first set of constraints are added to ensure that  $z$  takes the maximum value over  $g \in \mathcal{G}$ .

$$\begin{aligned}
& \min z \\
& \text{s. t. } \forall g \in \mathcal{G}, z \geq \frac{1}{K'(K'-1)} \sum_{k,l \in \mathcal{K}, k \neq l} \gamma_{kl} y_{kl}^g \\
& \forall k \in \mathcal{K} \quad \sum_{g=1}^G x_k^g = 1 \\
& \forall g \in \mathcal{G} \quad \sum_{k=1}^K x_k^g = K' \\
& \forall k, l \in \mathcal{K}, k \neq l, \forall g \in \mathcal{G} \quad y_{kl}^g \geq x_k^g + x_l^g - 1 \\
& \text{and } y_{kl}^g \leq x_k^g \text{ and } y_{kl}^g \leq x_l^g \\
& \forall k \in \mathcal{K}, \forall g \in \mathcal{G} \quad x_k^g \in \{0,1\} \\
& \forall k, l \in \mathcal{K}, k \neq l, \forall g \in \mathcal{G} \quad y_{kl}^g \in \{0,1\}
\end{aligned}$$

The above problem formulation assumes that each user group contains  $K' = M_t/M_r'$  users. For unequal group sizes, denote the size of group  $g$  by  $K_g$ . Then, the constant  $K'$  in the ILP problem can be replaced by  $K_g$  to accommodate unequal group sizes.



## CHAPTER 4

### SIMULATION RESULTS AND DISCUSSION

This chapter shows the simulation results of the research, which are divided into two simulation scenarios including single user MIMO-OFDM and multiuser MIMO in OWC systems, respectively.

#### 4.1 Single-User MIMO for an Indoor OWC System

This section presents numerical results obtained from analytical derivations and computer simulations, which correspond to the research objectives. The BER performances of the SVD-based MIMO-OFDM OWC systems are investigated and optimised under the impact of OFDM symbol design, the configuration of MIMO transmitters, the required data rates, the available bandwidth, and the angular diversity based on tilting receiver PDs.

##### 4.1.1 Simulation Parameters and Setups

This research focus on moderate data rates (below Gbps) so that commercial LED-based light sources, whose modulation bandwidth is limited to the order of 10 MHz, can be used. While there are techniques for increasing the modulation bandwidth of LEDs by an order magnitude, e.g., using pre-equalization circuits, it is not adopted to this research because the research would like to explore using multiple LEDs for MIMO transmissions without significantly increasing the transmitter hardware complexity.

Table 4.1: Simulation parameters for the SVD-based MIMO-OFDM OWC systems

Parameter	Notation	Value
Data rates	$R$	50, 100 Mbps
Transmit optical power	$P_T^{\text{total}}$	0-50 dBm
Number of OFDM subcarriers	$N$	64
Number of transmitted OFDM symbols	—	$10^2$
Maximum $M \times M$ -QAM constellation size	$M$	16
Lambertian order	$m$	1
LED semiangle	$\Phi_{1/2}$	$60^\circ$
Modulation index	$m_l$	1
PD responsivity	$\alpha_{A/W}$	0.53 A/W
PD field of view	$\Psi_c$	$70^\circ$
PD effective detection area	$A$	$1 \text{ cm}^2$
Target BER in bit loading	BER	$10^{-5}$

The number of OFDM subcarriers is set to 64, which is sufficiently large for indoor OWC. The constellation size is limited at 16x16-QAM which is typical for indoor OWC. The modulation index is assumed to be unity for simplicity and without loss of generality. The receiver responsivity follows a typical value mentioned in (Kahn and Barry,1997). Finally, the target BER is set to  $10^{-5}$ .

#### 4.1.2 Optimisation of OFDM Symbol

The question considered in this section is how to optimally design the OFDM symbol for the MIMO-OFDM system corresponding to the utilised BW and the data rate. In particular, the utilised BW of the system is quantified based on the number of bits per OFDM symbol, denoted by  $b_{\text{OFDM}}$ , as follows

$$BW = \frac{2RN}{b_{\text{OFDM}}} \quad (4.1)$$

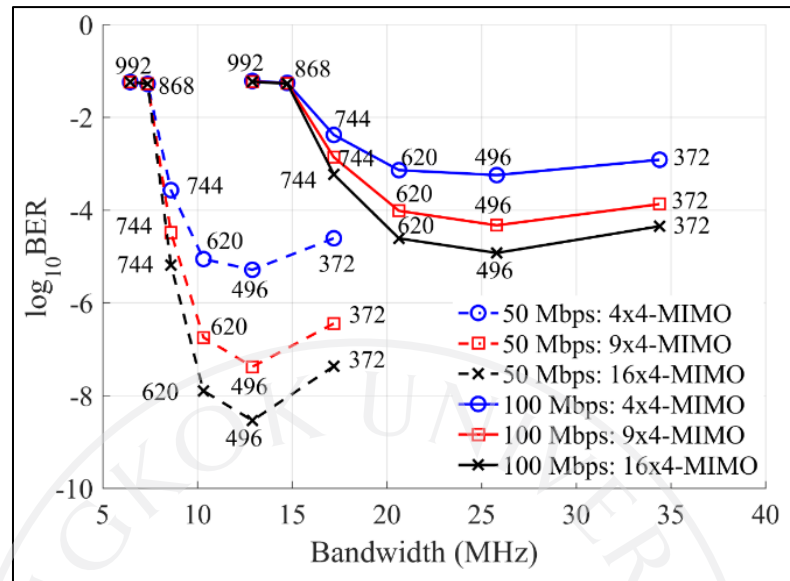


Figure 4.1: BER versus utilized BW (MHz) of  $4 \times 4$ -,  $9 \times 4$ - and  $16 \times 4$ -MIMO systems at R1: (2.5,2.5).

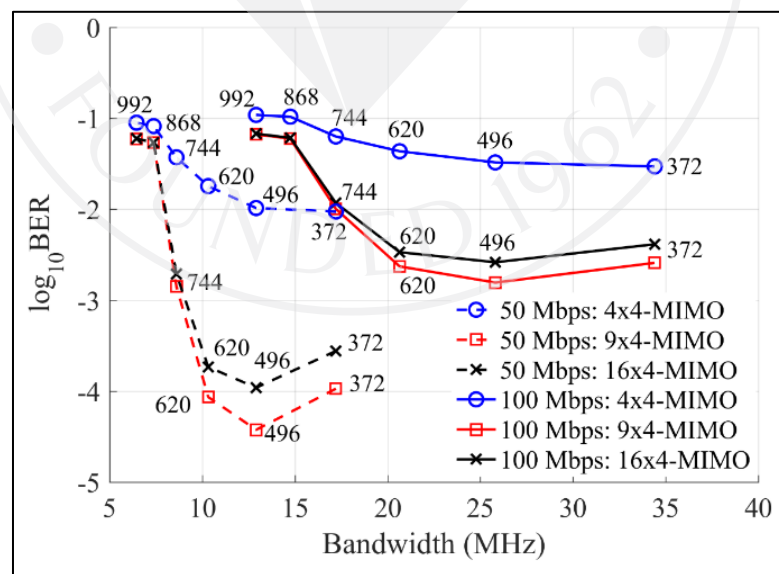


Figure 4.2: BER versus utilized BW (MHz) of  $4 \times 4$ -,  $9 \times 4$ - and  $16 \times 4$ -MIMO systems at R2: (1,1).

Then, for a certain data rate, the optimal BW is determined based on the BER performance, as shown in Figure 4.1 and Figure 4.2 that present the BER versus the utilised BW when the total power is  $P_T^{\text{total}} = 45 \text{ dBm}$  (31.6 W), the data rates are 50 and 100 Mbps, and the receiver positions are R1 and R2, respectively. In addition, this research investigates the optimal OFDM symbol design for all three MIMO configurations of  $4 \times 4$ ,  $9 \times 4$ , and  $16 \times 4$ . The values  $b_{\text{OFDM}} = 372, 496, 620, 744, 868, 992$  correspond to having on average 3, 4, 5, 6, 7, 8 bits per each of the 4 spatial channels on each subcarrier, respectively. For both receiver positions, it is seen that using  $b_{\text{OFDM}} = 496$  provides the optimal utilised BW at 12.9 MHz for the data rate of 50 Mbps and at 25.8 MHz for the data rate of 100 Mbps.

#### 4.1.3 MIMO Transmitter Configurations

In this section, using the optimal OFDM symbol design, i.e.,  $b_{\text{OFDM}} = 496$ , at the data rate of 50 Mbps, this research investigates the BER performance for different MIMO transmitter configurations. Figure 4.3 shows the BER versus the total transmit optical power for the three MIMO configurations ( $4 \times 4$ ,  $9 \times 4$ , and  $16 \times 4$ ) at receiver positions R1 and R2. Analytical results are plotted as lines while simulation results are plotted as markers. It is seen that there is a close match between analytical and simulation results. Obviously, the receiver position has a significant impact on the BER. At the BER of  $10^{-5}$ , the transmit power requirement increases by about 3 dB for the  $4 \times 4$  configuration when the receiver moves from R1 to R2.

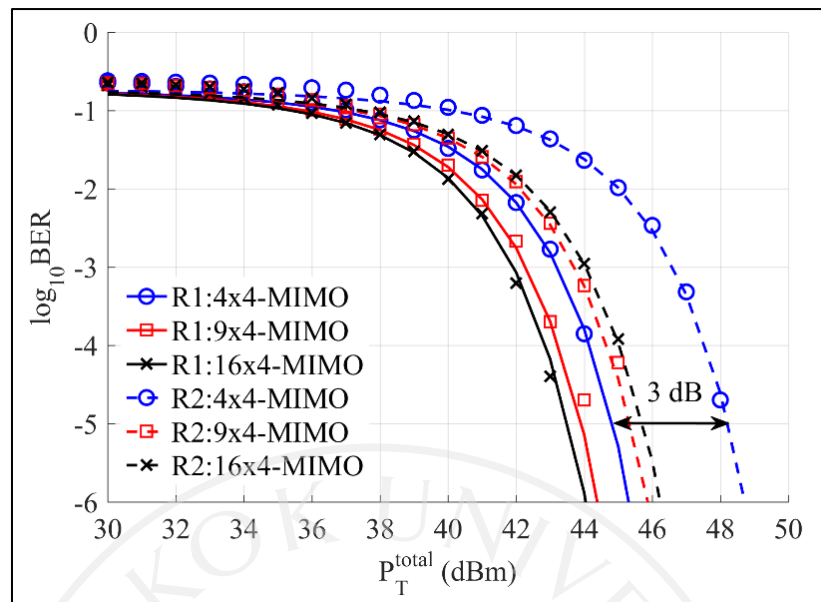


Figure 4.3: BER versus  $P_T^{\text{total}}$  of  $4 \times 4$ -,  $9 \times 4$ - and  $16 \times 4$ -MIMO systems at R1: (2.5,2.5) and R2: (1,1).

In addition, there are two important observations when the three MIMO configurations are compared. First, having more LEDs improves the system BER, and, clearly, the  $16 \times 4$  configuration offers the best performance. Nevertheless, the performance gain from  $9 \times 4$  versus  $4 \times 4$  is much larger than that of  $16 \times 4$  versus  $9 \times 4$ . Secondly, the power gain is more significant at R2, which is closer to the room corner. As the signal-to-noise ratio (SNR) increases while the noise power remains constant in the system model, the total transmit optical power increases. It can be seen from Figure 4.3 that an increase in the SNR or the transmit power will reduce the BER.

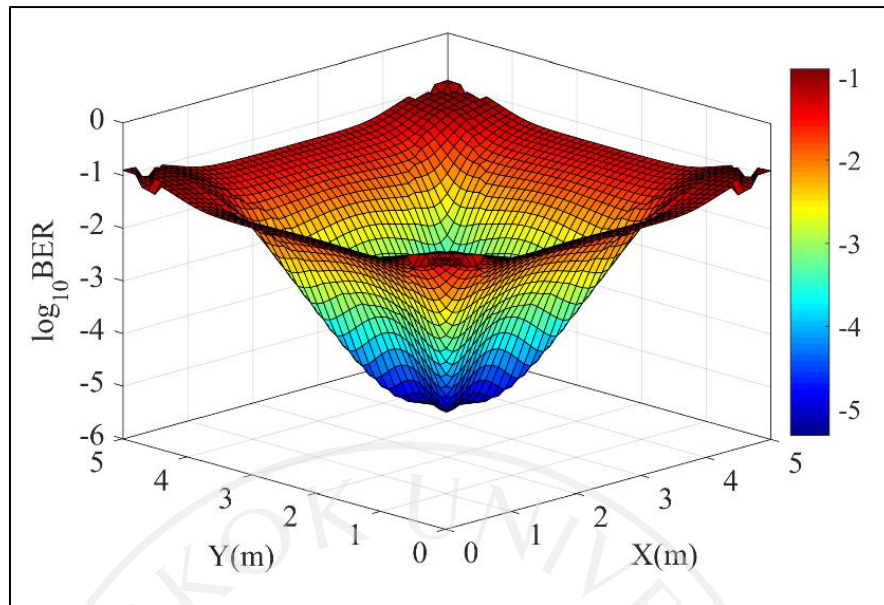


Figure 4.4: 3D plot of BER of  $4 \times 4$ -MIMO with  $P_T^{\text{total}} = 45$  dBm.

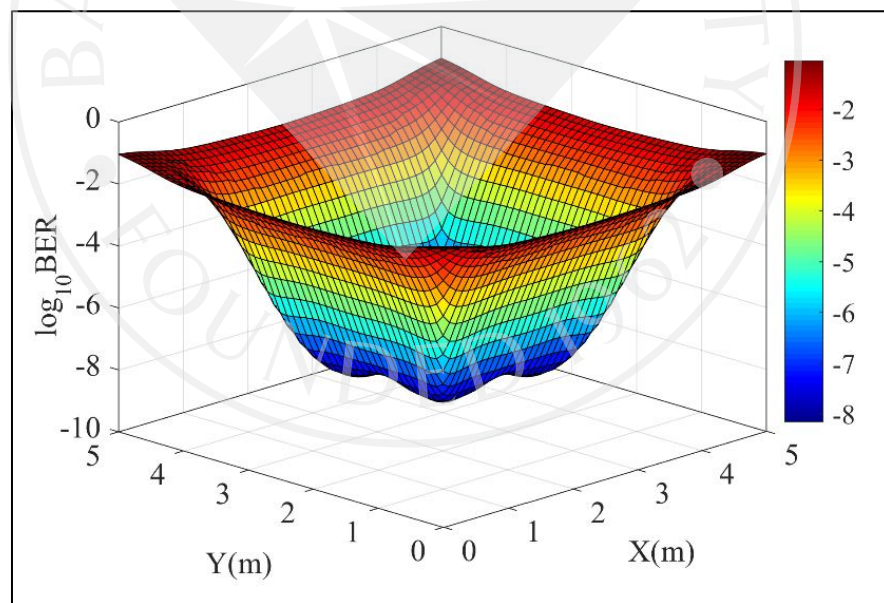


Figure 4.5: 3D plot of BER of  $9 \times 4$ -MIMO with  $P_T^{\text{total}} = 45$  dBm.

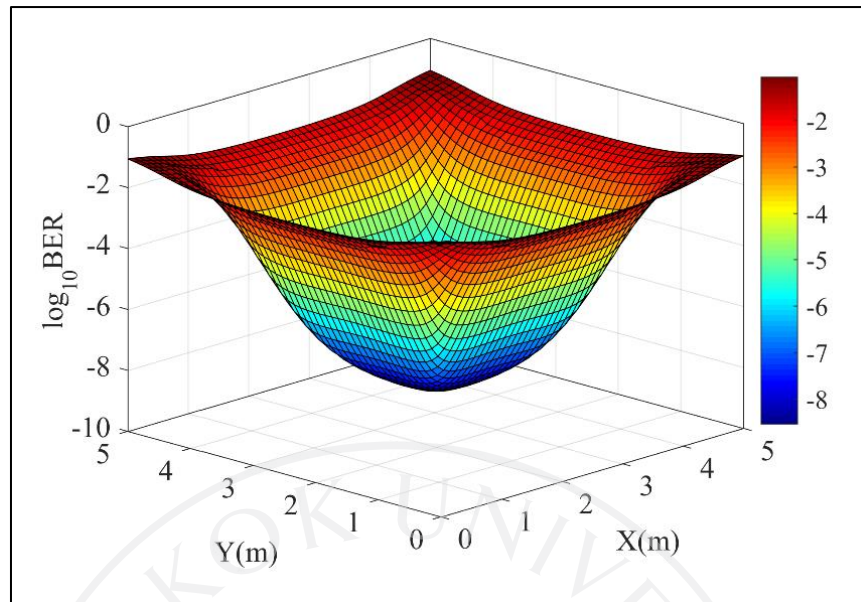


Figure 4.6: 3D plot of BER of  $16 \times 4$ -MIMO with  $P_T^{\text{total}} = 45$  dBm.

Figure 4.4 - Figure 4.6 compare the BER distribution in the room for the three MIMO configurations of  $4 \times 4$ ,  $9 \times 4$ , and  $16 \times 4$ , respectively. The BER is computed for a grid of receiver positions with the grid spacing of 0.1 m, yielding  $51 \times 51$  receiver positions within the given room. The total transmit power of 45 dBm is used for all configurations. The 3D BER plots in Figure 4.4 - Figure 4.6 show that low BERs  $10^{-3}$  can be achieved in many more positions using  $9 \times 4$  and  $16 \times 4$  configurations in comparison to using the  $4 \times 4$  configuration. This fact is more clearly demonstrated by the cumulative distribution function (CDF) of the BER for all three configurations in Figure 4.7. It is seen that, in 50% of the positions, the BER of less than  $10^{-3}$  can be achieved for both  $9 \times 4$  and  $16 \times 4$  configurations while the number is only 20% for the  $4 \times 4$  configuration.

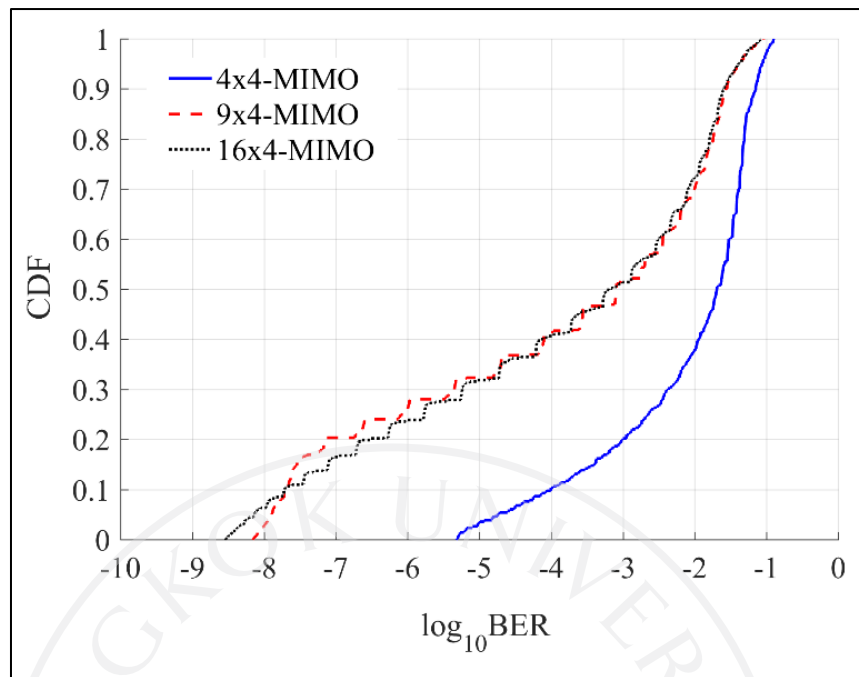


Figure 4.7: CDF of BER of 4x4-, 9x4-, and 16x4-MIMO systems with  $P_T^{\text{total}} = 45$  dBm.

It is also observed that 9x4 and 16x4 configurations have very similar BER distributions while the 9x4 one requires relatively lower computational complexity. The research will therefore further investigate this configuration in the following sections.

#### 4.1.4 Polar Angle Tilting of PDs and Dimming Control

This section analyses the impact of polar angle tilting of PDs in the 4x4 and 9x4 configurations. Figure 4.8 shows the BER versus the tilting polar angle of the receive PDs, denoted by  $\theta_R$ , at the total transmit optical power of 40 dBm (10 W). It is seen in both configurations that the BER can be improved at any position by increasing the tilting polar angle. As evident from Figure 4.8, the BER at R2 in the 9x4 system can be improved from  $10^{-1}$  (unacceptable) to  $10^{-5}$  and  $10^{-8}$  with the tilting angle of  $2^\circ$  and  $3^\circ$ , respectively.



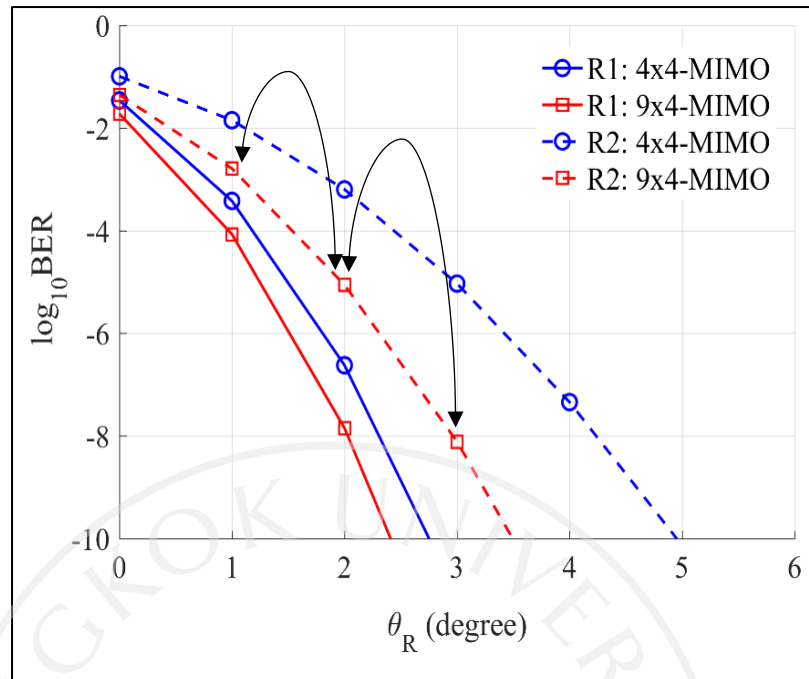


Figure 4.8: BER versus polar angle of 4x4- and 9x4-MIMO systems with  $P_T^{\text{total}} = 40$  dBm.

In addition, Figure 4.9 and Figure 4.10 illustrate the BER versus the required total transmit optical power. It is seen that, with the tilting angle of  $1^\circ$  and  $5^\circ$ , the required total power of 9x4-MIMO is less than that for 4x4-MIMO without tilting by approximately 4 dB and 9 dB at the BER of  $10^{-5}$ , respectively. The gains are approximately 6 dB and 12 dB, respectively, for the receiver at R2, as shown in Figure 4.10.

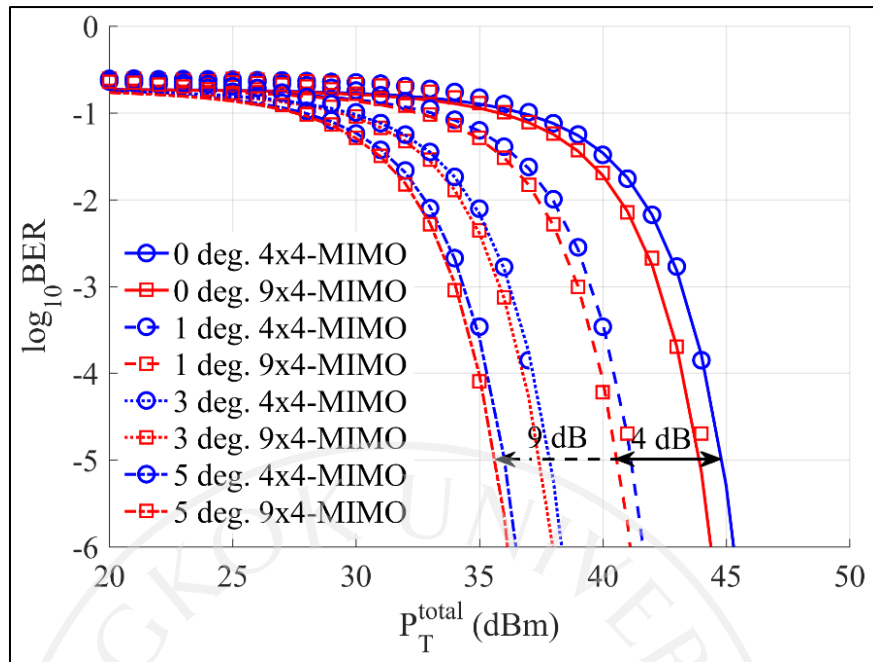


Figure 4.9: BER versus  $P_T^{\text{total}}$  for tilting polar angles of PDs for 4x4- and 9x4-MIMO at R1: (2.5,2.5).

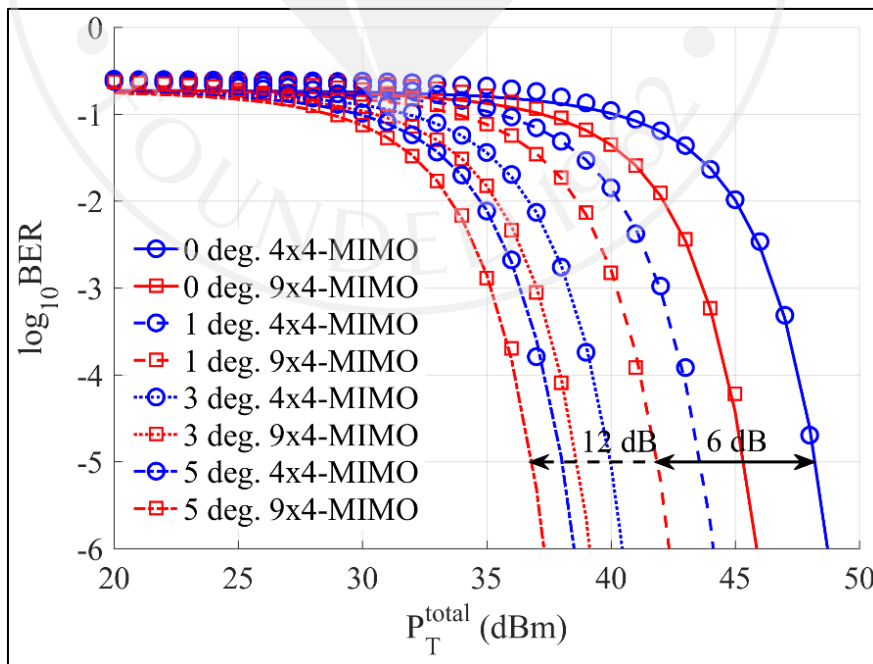


Figure 4.10: BER versus  $P_T^{\text{total}}$  for tilting polar angles of PDs for 4x4- and 9x4-MIMO at R2:(1,1).

The above observation suggests that it is possible to use polar angle tilting in case of light dimming with a low transmit power, e.g.,  $P_T^{\text{total}}$  can be as low as 1 W (30 dBm). As shown in Figure 4.11 and Figure 4.12, we can adjust the tilting polar angle at both receiver positions to achieve an operational BER ( $10^{-5}$ ) with the data rate of 50 Mbps in both 4×4- and 9×4-MIMO configurations when the total power is as low as 0.5 W (27 dBm). The discontinuity in the BER curves indicate that  $\text{BER} \leq 10^{-10}$  is obtained. This considered scenario ensures reliable data transmissions under all illumination conditions since the additional DC bias does not affect the communication system performance. Therefore, data communications can be supported even in dark rooms.

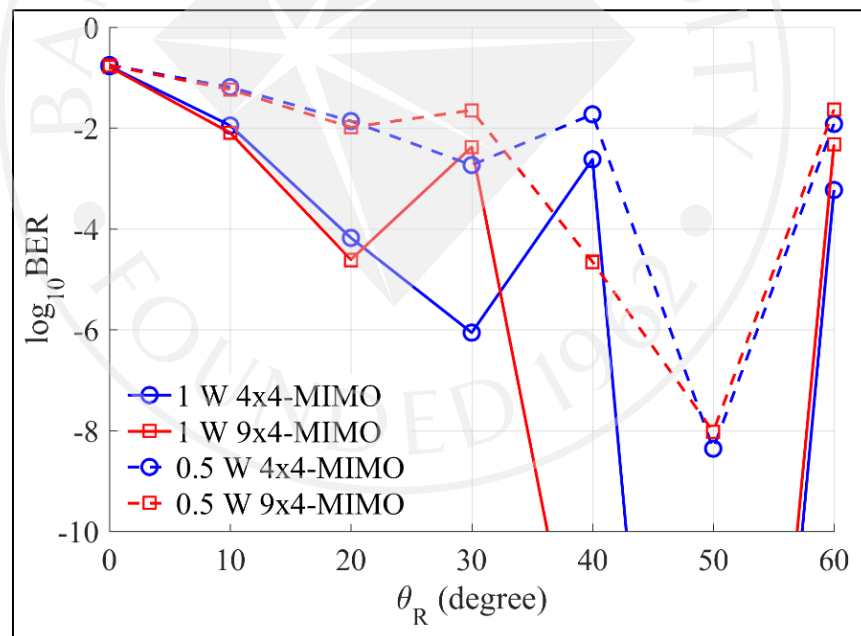


Figure 4.11: BER versus polar angle of 4×4- and 9×4-MIMO systems with

$$P_T^{\text{total}} = 30 \text{ dBm and } P_T^{\text{total}} = 27 \text{ dBm at R}_1: (2.5, 2.5).$$

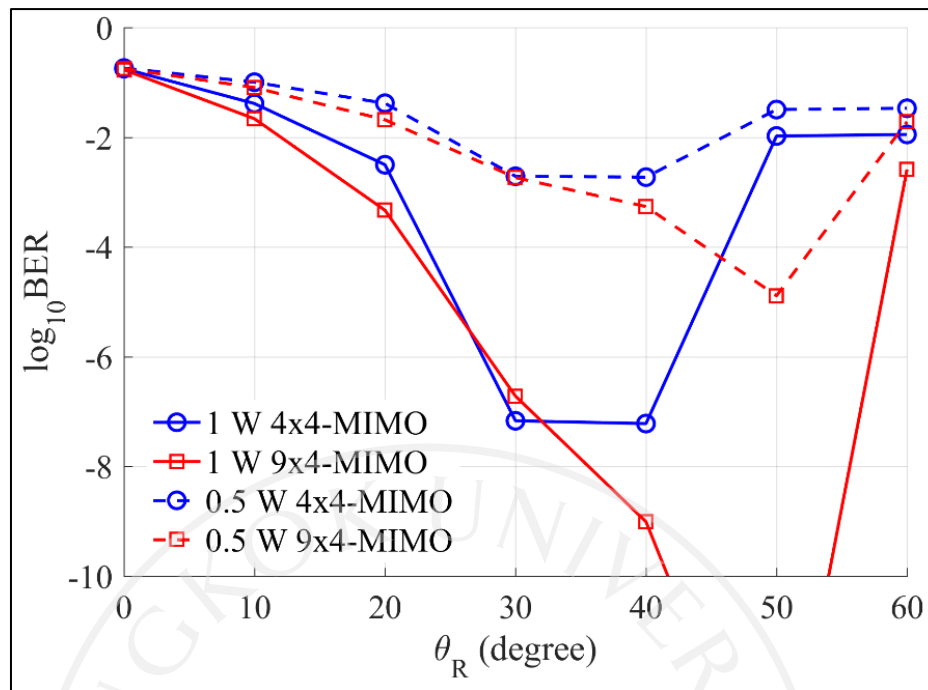


Figure 4.12: BER versus polar angle of 4x4- and 9x4-MIMO systems with

$$P_T^{\text{total}} = 30 \text{ dBm and } P_T^{\text{total}} = 27 \text{ dBm at R2: (1,1).}$$

The impact of the polar angle tilting on the improvement of BER performance can be explained using Table 4.2, which shows the condition numbers of the 4x4-, 9x4- and 16x4-MIMO channel matrices with various polar angles of PDs.

Note that, the condition number can be calculated as  $\sigma_{\max}/\sigma_{\min} \geq 1$ , where  $\sigma_{\max}$  is the largest singular value and  $\sigma_{\min}$  is the smallest singular value in  $\Sigma_k$ .

The singular values or spatial channel gains, i.e.,  $\sigma_{1,k}, \dots, \sigma_{L_k,k}$ , from the diagonal entries of  $\Sigma_k$  in (3.1) for the 4x4-, 9x4-, and 16x4-MIMO systems are shown in  $\Sigma_k$  below.

$$\Sigma_k = \begin{bmatrix} \sigma_{1,k} & 0 & \dots & 0 & \dots & 0 \\ 0 & \sigma_{2,k} & \dots & 0 & \dots & 0 \\ \vdots & \vdots & \ddots & \vdots & \ddots & \vdots \\ 0 & 0 & 0 & \sigma_{L_k,k} & \dots & 0 \end{bmatrix}$$

The results show that the system can obtain a high multiplexing gain (with low condition numbers) with large polar angles of PDs. Nevertheless, operating with large

tilting angles leaves smaller margins (with respect to the PD FOV) for movement of receiver units, and may be appropriate only when little movement is expected, which is usually the case in dark rooms.

#### 4.1.5 Computational Complexity

According to Figure 3.5 and Figure 3.6, there is hardware computation complexity due to IDFT computation at the transmitter site. Because each transmit LED requires one  $N$ -point IDFT module, the number of the required IDFT modules in  $M_t \times M_r$ -MIMO flip-OFDM increases linearly with  $M_t$ . In addition, the time complexity of SVD is  $O(mn^2)$ , where  $m \geq n$ , and  $m/n$  is the number of columns/rows in the MIMO channel matrix. In the considered scenarios,  $m = M_t$  and  $n = M_r$ , yielding the time complexity of  $O(M_t M_r^2)$ . Hence, there is a tradeoff between the computational complexity and the BER performance.

Table 4.2: The condition numbers of 4×4-, 9×4-, and 16×4-MIMO channel matrices for various tilting polar angles of PDs

Receiver position	$M_t \times M_r$ -MIMO	0°	1°	3°	5°	10°	30°	50°
R1:(2.5,2.5)	4×4-MIMO	$2.1401 \times 10^4$	$7.7286 \times 10^3$	$3.3907 \times 10^3$	$2.1688 \times 10^3$	$1.1339 \times 10^3$	7.1349	98.9977
	9×4-MIMO	$5.1300 \times 10^4$	$1.8525 \times 10^4$	$8.1266 \times 10^3$	$5.1976 \times 10^3$	$2.7168 \times 10^3$	19.1206	212.1289
	16×4-MIMO	$4.5398 \times 10^4$	$1.8072 \times 10^4$	$8.1757 \times 10^3$	$5.2742 \times 10^3$	$2.7770 \times 10^3$	27.9164	20.4013
R2:(1,1)	4×4-MIMO	$4.4752 \times 10^5$	$9.4171 \times 10^4$	$3.6811 \times 10^4$	$2.2859 \times 10^4$	$1.1663 \times 10^4$	$2.3550 \times 10^4$	22.1358
	9×4-MIMO	$9.8249 \times 10^4$	$3.5396 \times 10^4$	$1.5625 \times 10^4$	$1.0019 \times 10^4$	$5.2514 \times 10^3$	45.2626	19.7535
	16×4-MIMO	$9.4038 \times 10^4$	$3.6313 \times 10^4$	$1.6300 \times 10^4$	$1.0494 \times 10^4$	$5.5184 \times 10^3$	46.2788	16.0005

## 4.2 Multiuser MIMO for an Indoor OWC System

This section shows the numerical performance results of the efficient user grouping for MU-MIMO OWC based on block diagonalization.

### 4.2.1 Simulation Parameters and Setups

For numerical results, consider a room with the dimension of  $5\text{m} \times 5\text{m} \times 2.5\text{m}$ . The simulation parameters are set as Table 4.3. For simplicity, the number of PDs for user is set to 2, but the same grouping techniques are also valid for a higher number of PDs, e.g., 4.

Table 4.3: Simulation parameters for MU-MIMO OWC systems

Parameter	Notation	Value
Number of LED transmitters	$M_t$	4,6,8
Number of users	$K$	4,6,8
Number of PDs per user	$M'_r$	2
Lambertian order	$m$	1
Modulation index	$m_l$	1
PD responsivity	$\alpha_{A/W}$	0.53 A/W
PD field of view	$\Psi_{\text{FOV}}$	$70^\circ$
PD effective detection area	$A$	$1 \text{ cm}^2$
The effective path losses	$\sigma_{k,n}$	$10^{-6}$
The signal to noise ratio	$K_{\text{SNR}}\sigma_{k,n}^2$	10, 15, 20 dB

For each value of  $M_t$  (number of LED transmitters) and  $K_{\text{SNR}}$  (SNR parameters), 1,000 random scenarios of user locations are generated. The average minimum user throughputs are evaluated from the three methods of user grouping, the hybrid method (choosing the best answer of the three methods), and exhaustive search. Note that exhaustive search always provides optimal user grouping, but the associated computational complexity is too high for large numbers of LED transmitters and users. For convenience, the three methods are called method 1 ( $D_{kl}$  maximize the minimum distance), method 2 ( $R_{kl}$  minimize the maximum correlation coefficient), and method 3 ( $N_{kl}$  maximize the minimum normalized matrix norm of its projection on the other user's nullspace). In what follows, the SNRs of 10, 15, and 20 dB will be referred to as low, medium, and high SNRs, respectively.

The transmitter locations are shown in Figure 4.13. User locations are randomly and uniformly generated to be anywhere in the room. Their PDs are located at a fixed height of 0.8 m. The PDs of each user are equally separated on the radius- $\varepsilon$  circle centered at the user location, where  $\varepsilon = 1$  cm and the first PD is equally likely to be anywhere on the circle. For each PD of each user, assume that  $A = 1 \text{ cm}^2$  and  $\Psi_{\text{FOV}} = 70^\circ$ .

#### 4.2.2 Example User Grouping Scenarios

This section shows the examples of user grouping in terms of minimum user throughput (bit/s/Hz). There are four LED transmitters are located as Figure 4.13 (a). The numerical results are divided into two simulation scenarios, where the four users of each scenario are located as shown in Figure 4.14. In addition, the user and PD locations of these two scenarios are shown in Table 4.4 and Table 4.5, respectively.



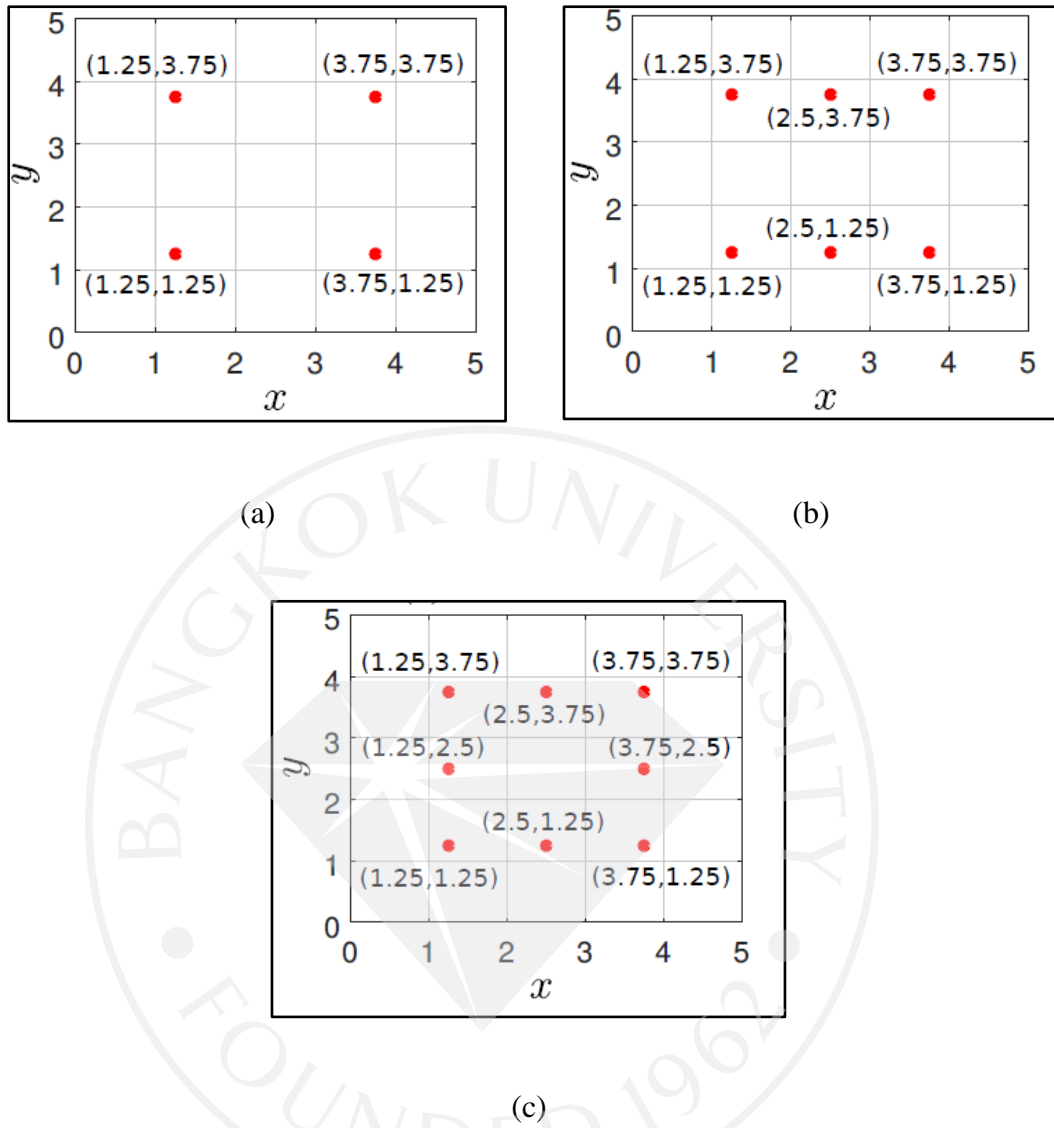


Figure 4.13: Bird's eye view of LED transmitter locations for (a) scenarios with 4 transmitters, (b) scenarios with 6 transmitters, and (c) scenarios with 8 transmitters

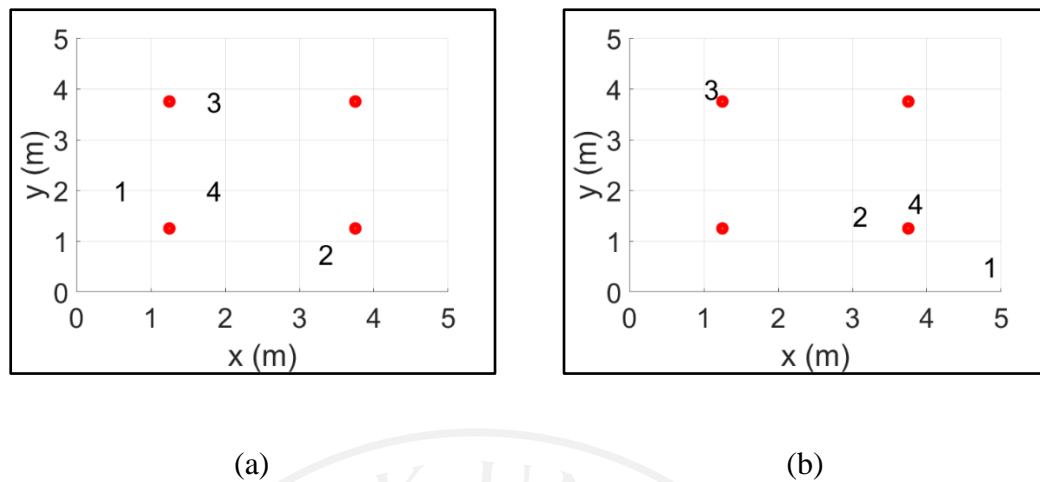


Figure 4.14: Bird's eye view of user locations shown as digits and transmitter locations shown as dots (a) scenario 1, (b) scenario 2.

Table 4.4: User and PD locations for scenario 1

User	Location	PD locations on radius- $\epsilon$ circle
1	(0.5, 2, 0.8)	$0^\circ, 180^\circ$
2	(3.25, 0.75, 0.8)	$45^\circ, 225^\circ$
3	(1.75, 3.75, 0.8)	$90^\circ, 270^\circ$
4	(1.75, 2, 0.8)	$135^\circ, 315^\circ$

Note that the angle  $0^\circ$  points towards the positive x-axis. For the throughput evaluations using (3.32), assume that  $K_{\text{SNR}}$  in (3.33) is such that the receiver signal-to-noise ratio (SNR), which is  $K_{\text{SNR}}\sigma_{k,n}^2$ , is equal to 15 dB for typical path loss  $\sigma_{k,n} = 10^{-6}$ . In other words,  $K_{\text{SNR}} \approx 3.1623 \times 10^{13}$ .

Table 4.5: User and PD locations for scenario 2

User	Location	PD locations on radius- $\epsilon$ circle
1	(4.75, 0.5, 0.8)	60°, 240°
2	(3, 1.5, 0.8)	120°, 300°
3	(1, 4, 0.8)	100°, 280°
4	(3.75, 1.75, 0.8)	105°, 285°

In particular, there are four LED transmitters and four users each with two PDs, i.e.,  $M_t = 4$ ,  $K = 4$ , and  $M_r' = 2$ . To apply BD precoding, users need to be divided into two groups each with two users, i.e.,  $K' = 2$ . According, the numerical results are shown as below.

Table 4.6: Minimum user throughputs for scenario 1

User grouping	Minimum user throughput (bit/s/Hz)
{1,2} and {3,4}	2.84
{1,3} and {2,4}	3.63
{1,4} and {2,3}	2.78

Table 4.6 lists all three possible user groupings as well as the corresponding minimum user throughputs based on the computation using (3.32). From the throughputs, the best-case grouping yields the minimum throughput (3.63 bit/s/Hz) that is 1.31 times the value for the worst-case grouping (2.78 bit/s/Hz).

Table 4.7: Minimum user throughputs for scenario 2

User grouping	Minimum user throughput (bit/s/Hz)
{1,2} and {3,4}	1.58
{1,3} and {2,4}	3.54
{1,4} and {2,3}	0.63

Table 4.7 lists all three possible user groupings as well as the corresponding minimum throughputs. From the throughputs, the best-case grouping yields the minimum throughput (3.54 bit/s/Hz) that is as high as 5.62 times the value for the worst-case grouping (0.63 bit/s/Hz).

The two example scenarios demonstrate that efficient user grouping can help increase the minimum user throughputs significantly compared to the worst-case values. The next section discusses the numerical results of the proposed methods for user grouping.

#### 4.2.3 Average Minimum User Throughputs

This section shows the average minimum user throughput for different methods of user grouping for scenarios with  $M_t = 4$ ,  $K = 4$ , and  $M_r = 2$ , where the transmitter locations are located as shown in Figure 4.13 (a). The results are plotted in Figure 4.15.

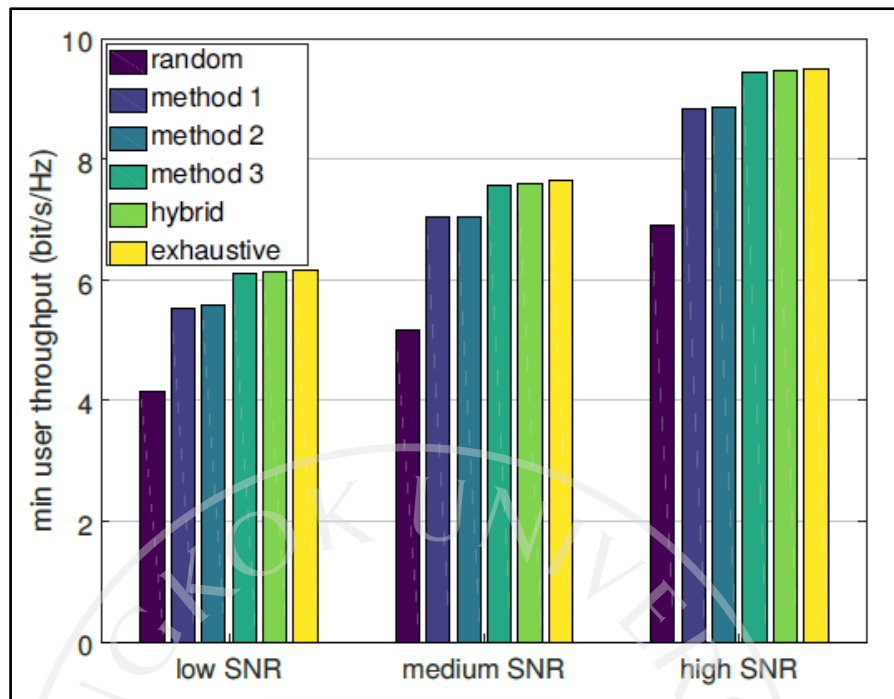


Figure 4.15: Average minimum user throughputs for scenarios with  $M_t = 4$ ,  $K = 4$ , and  $M_r' = 2$ .

It can be seen that random grouping is significantly less efficient than other methods. Method 3 performs the best among the proposed 3 methods. In addition, method 3 performs close to the hybrid method and exhaustive search. The relative performances are similar for low, medium, and high SNR values.

Figure 4.16 shows the average minimum user throughputs for different methods of user grouping for scenarios with  $M_t = 6$ ,  $K = 6$ , and  $M_r' = 2$ . Similar to Figure 4.15, random grouping is significantly less efficient than other methods. While method 3 still outperforms methods 1 and 2, there is now a noticeable gap between method 3 and the hybrid method, and also between the hybrid method and exhaustive search.

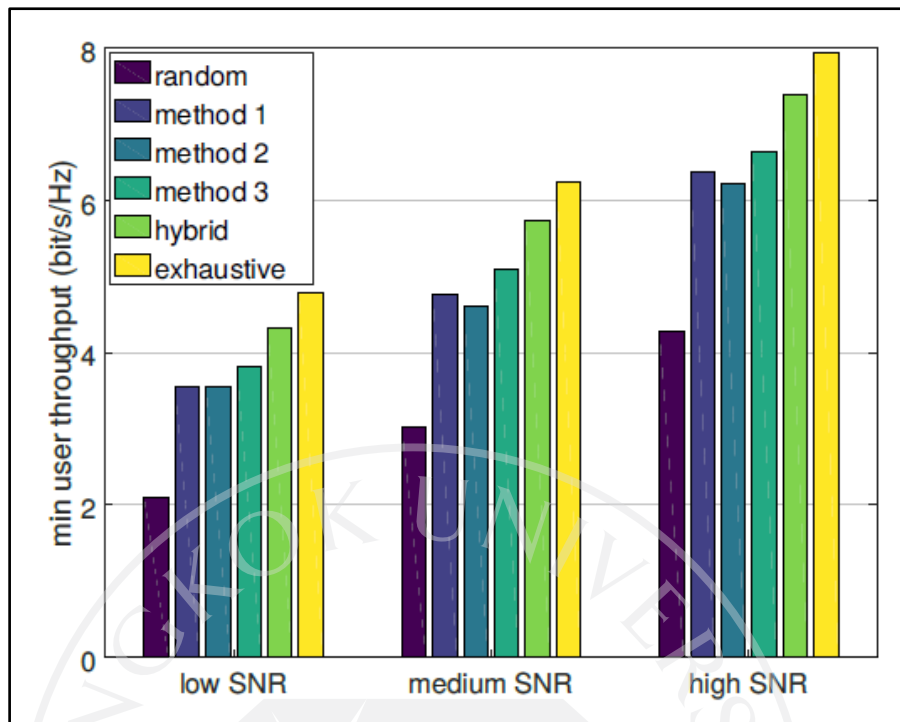


Figure 4.16: Average minimum user throughputs for scenarios with  $M_t = 6, K = 6$ , and  $M_r' = 2$ .

The fact that method 3 and the hybrid approach cannot perform as well as exhaustive search in Figure 4.16 is because the proposed user grouping methods consider pairwise interferences among users. When the user group size is  $K' = M_t/M_r' = 6/2 = 3$ , optimal grouping will need to consider mutual interferences among three users instead of pairwise interference only. Nevertheless, the hybrid method performs much better than random grouping, and performs reasonably efficient compared to optimal grouping from exhaustive search. In particular, the throughputs of the hybrid method are 90.4%, 91.9%, and 93.1% of the values from exhaustive search for low, medium, and high SNR scenarios, respectively.

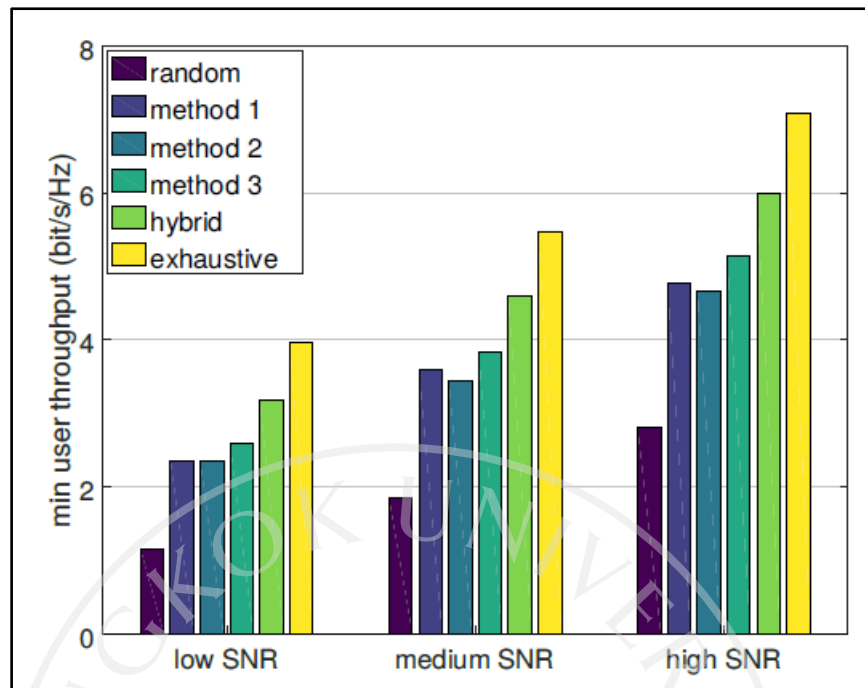


Figure 4.17: Average minimum user throughputs for scenarios with  $M_t = 8, K = 8$ , and  $M'_r = 2$ .

Figure 4.17 shows the average minimum user throughputs for different methods of user grouping for scenarios with  $M_t = 8, K = 8$ , and  $M'_r = 2$ . Similar to Figure 4.15 and Figure 4.16, random grouping is significantly less efficient than other methods. Similar to Figure 4.16, method 3 outperforms methods 1 and 2, but is less efficient than the hybrid method, which in turn is less efficient than exhaustive search. Nevertheless, the hybrid method performs reasonably well, with the throughputs equal to 81.1%, 83.3%, and 85.9% of the values from exhaustive search for low, medium, and high SNR scenarios, respectively.

Recall that, for each SNR scenario in Figure 4.15 to Figure 4.17, we simulated 1,000 random scenarios of user locations. Based on these simulation results, Table 4.8 shows the percentages of random scenarios in which method 1, method 2, and

method 3 are chosen by the hybrid method. It can be seen that all methods are used at least 10% of the time for each system configuration.

Table 4.8: Percentages of random scenarios in which each method is chosen by the hybrid method

$(M_t, K, M_r')$	SNR	Method		
		1	2	3
(4,4,2)	low	65.2%	12.9%	21.9%
	medium	67.2%	11.6%	21.2%
	high	62.8%	12.7%	24.5%
(6,6,2)	low	52.4%	23.0%	24.6%
	medium	53.0%	23.7%	23.3%
	high	49.7%	26.0%	24.3%
(8,8,2)	low	43.7%	27.1%	29.2%
	medium	44.4%	28.4%	27.2%
	high	44.4%	30.0%	25.6%

#### 4.2.4 Comparison of Computational Complexity

To compare the computational complexity between the hybrid method and the exhaustive method, for each value of  $(M_t, K, M_r')$ , we simulate 20 random scenarios of user and PD locations and compute the average run time taken by each method. Table 4.9 compares the average run times using GNU Octave on a laptop computer with a Core i7 Intel processor and 8 GB of RAM. In particular, the command `glpk` in



Octave is used to solve ILP problems for the hybrid method. It can be seen that, as the problem size increases (i.e., increasing  $K$ ), the average run time of the hybrid method becomes significantly lower than that of the exhaustive method.

Table 4.9: Average run times for the hybrid method and the exhaustive method

$(M_t, K, M'_r)$	Method	
	Hybrid	Exhaustive
(6,6,2)	0.0217 s	0.0102 s
(6,8,2)	0.0908 s	0.0462 s
(6,10,2)	0.358 s	0.444 s
(6,12,2)	1.72 s	9.89 s

#### 4.2.5 User Grouping for Throughput Improvements when $M_r \leq M_t$

This section considers user grouping when  $M_r \leq M_t$ , which corresponds to scenarios in which all users could be supported as a single group using BD precoding. However, numerical results indicate that user grouping, while unnecessary for BD precoding, can help improve the average minimum user throughputs.

In particular, consider scenarios with  $M_t = 8, K = 4$ , and  $M'_r = 2$ . Four grouping schemes are compared in what follows. The first scheme puts all four users in a single group and applies BD precoding. The other three schemes separate users into two groups of two users, with user grouping based on the random method, the proposed hybrid method, and exhaustive search, respectively. For fair comparison, when computing the user throughput using (3.32), a factor of  $1/2$  is multiplied to each

user throughput in the last three schemes since TDM with two timeslots is applied to support two user groups.

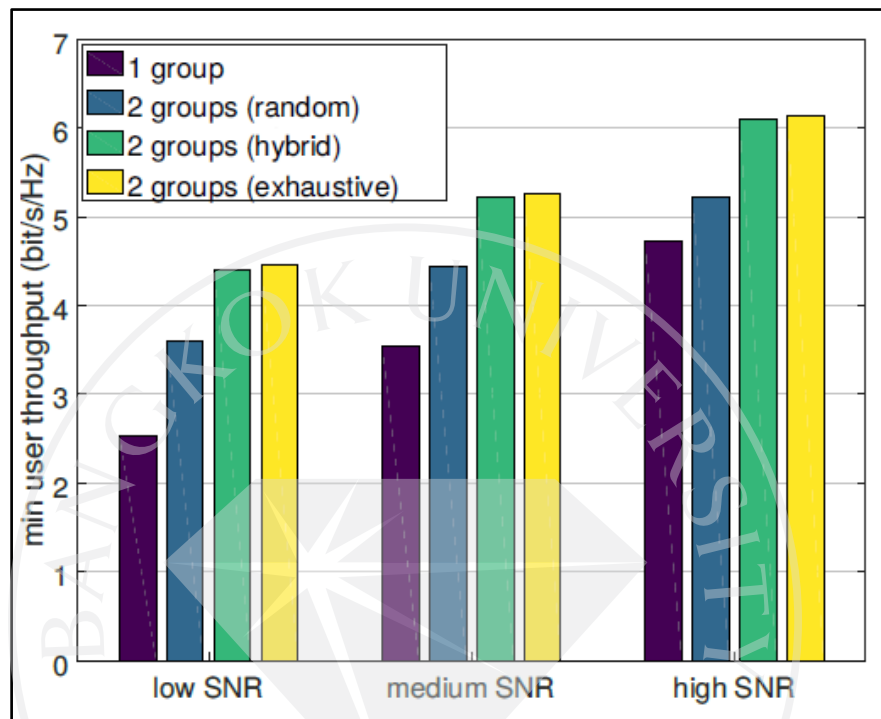


Figure 4.18: Average minimum user throughputs for scenarios with  $M_t = 8$ ,  $K = 4$ , and  $M_r' = 2$ .

Figure 4.18 shows the average minimum user throughputs obtained from the four schemes in low, medium, and high SNR scenarios. It can be seen that, with 4 users in a single group, the minimum user throughputs are lower than the values for two groups of two users, even with random user grouping. This is because BD precoding completely prevents interference among users by projecting each user's signals onto the null space of all the other users' signals, yielding possibly high attenuation of desired user signals in the process. Compared to random user grouping, the proposed hybrid method can further improve the throughputs.

In addition, the throughputs from the proposed hybrid method are close to the values from exhaustive search. The above results indicate that efficient user grouping can possibly benefit even for scenarios with  $M_r \leq M_t$ , which in principle does not require user grouping to operate BD precoding. Hence, when the number of users becomes high, efficient user grouping should be considered while operating MU-MIMO VLC systems with BD precoding.



## CHAPTER 5

### CONCLUSION AND RECOMMENDATIONS

In the first half, this research presents a detailed analysis of SVD based MIMO flip-OFDM and investigates the BER performances of transmitter distributions as well as tilting polar angles of receiver PDs in order to improve the channel diversity. For a given number of bits per OFDM symbol, the transmission performances are evaluated in terms of the BER versus the transmit optical power. By varying the number of bits per OFDM symbol, which specifies the utilised BW, numerical results show that optimal utilised BWs are 12.9 MHz for the data rate of 50 Mbps and 25.8 MHz for the data rate of 100 Mbps, with 496 bits per OFDM symbol in both cases. In addition, given the same total transmit optical power, the 9×4-MIMO system is shown to be optimal since it provides better BER performances compared to the 4×4-MIMO system, and requires lower computational complexity compared to the 16×4-MIMO system.

Moreover, with small tilting polar angles of PDs, i.e., 1° to 5°, the BER performances of 4×4- and 9×4-MIMO systems improve further. Finally, in case of low transmit optical powers, i.e.,  $P_T^{\text{total}} \leq 30$  dBm, 4×4- and 9×4-MIMO systems can still provide good BER performances at large tilting polar angles of PDs as high as 50°.

With improvement of the BER performance across different locations throughout the room, the indoor OWC system can better support mobility in multimedia streaming since good signal quality can be obtained almost everywhere within the room.

Furthermore, the large tilting angle can provide benefits in terms of the high multiplexing gains as indicated by improved condition numbers of MIMO channel matrices.

In the second half, this research is further extended to user grouping for MU-MIMO OWC systems with BD precoding. User grouping is investigated so that BD precoding can be applied to scenarios with a large number of users through the use of TDM timeslots. Three different user grouping methods as well as the hybrid method are proposed and compared with random user grouping and exhaustive search. Numerical results on the average minimum user throughputs over random scenarios of user locations indicate that the proposed hybrid method can significantly outperform random user grouping, and performs reasonably well compared to exhaustive search.

In particular, in a  $5\text{m}\times 5\text{m}\times 2.5\text{m}$ . room with 4, 6, and 8 LED transmitters with 4, 6, and 8 users each with 2 PDs, the proposed hybrid user grouping method can provide at least 80% of the throughputs provide by optimal grouping through exhaustive search in all scenarios. Finally, for scenarios with 8 LED transmitters and 4 users each with 2 PDs, it is demonstrated that user grouping can help improve the minimum user throughputs even though BD precoding can simultaneously support all users. Therefore, the proposed user grouping method can be useful for operating MU-MIMO OWC systems with BD precoding when the number of users in the same room becomes large.

For future works, further investigations on when to divide users into smaller groups for throughput improvement are recommended. In addition, user grouping can also be investigated under other precoding schemes for MU-MIMO OWC.

## BIBLIOGRAPHY

- Afgani, M.Z., Haas, H., Elgala, H., & Knipp, D. (2006). Visible light communication using OFDM. *Proceedings of 2nd International Conference on TRIDENTCOM 2*. Spain.
- Al-Ahmadi et al.(2018). Multi-User Visible Light Communications: State-of-the-Art and Future Directions. *Journal of IEEE Access*, 6, 70555-70571.
- Armstrong, J., & Lowery, A.J. (2006). Power efficient optical OFDM. *Electronics Letters*, 42(6), 370-372.
- Armstrong, J., & Schmidt, B.J.C. (2008). Comparison of asymmetrically clipped optical OFDM and DC-biased optical OFDM in AWGN. *IEEE Communications Letters*, 12(5), 343-345.
- Armstrong, J. (2009). OFDM for Optical Communications. *Journal of Lightwave Technology*, 27(3), 189-204.
- Bolcskei, H. (2006). MIMO-OFDM wireless systems: basics, perspectives, and challenges, *IEEE Wireless Communications*, 13(4), 31-37.
- Butala, P. M., Elgala, H., & Little, T. D. C. (2013). SVD-VLC: A novel capacity maximizing VLC MIMO system architecture under illumination constraints, *Proceedings of IEEE Globecom Workshops*, USA.
- Chen, J., & Hong, Y., & Wang, Z., & Yu, C. (2013). Precoded visible light communications. *Proceedings of Information, Communications & Signal Processing*, Tainan.

- Chen, J., & Ma, N., & Hong, Y., & Yu, C. (2014). On the performance of MU-MIMO indoor visible light communication system based on THP algorithm. *Proceedings of IEEE/CIC International Conference on Communications, China*.
- Czink et al. (2009). Spatial separation of multi-user MIMO channels. *Proceedings of IEEE 20th International Symposium on Personal, Indoor and Mobile Radio Communications, Japan*.
- Dissanayake, S.D., & Armstrong, J. (2013). Comparison of ACO-OFDM, DCO-OFDM and ADO-OFDM in IM/DD Systems. *Journal of Lightwave Technology*, 31(7), 1063-1072.
- Elgala, H., Mesleh, R., Haas, H., & Pricope, B. (2007). OFDM visible light wireless communication based on white LEDs. *Proceedings of IEEE 65th Vehicular Technology Conference, Ireland*.
- Elgala, H., Mesleh, R., & Haas, H., (2009). Indoor broadcasting via white LEDs and OFDM. *IEEE Transactions on Consumer Electronics*, 55(3), 1127-1134.
- Fath, T., & Haas, H. (2013). Performance Comparison of MIMO Techniques for Optical Wireless Communications in Indoor Environments. *IEEE Transactions on Communications*, 61(2), 733-742.
- Fernando, N., Hong, & Viterbo, E. (2011). Flip-OFDM for optical wireless communications. *Proceedings of IEEE Information Theory Workshop, Brazil*.
- Fernando, N., Hong, & Viterbo, E. (2012). Flip-OFDM for Unipolar Communication Systems. *IEEE Transactions on Communications*, 60(12), 3726-3733.
- Ghassemlooy et al. (2016). Effect of optimal Lambertian order for cellular indoor optical wireless communication and positioning systems. *Optical Engineering, SPIE*, 55(6).

- Ghassemlooy, Z., Popoola W., & Rajbhandari, S. (2017). *Optical Wireless Communications: System and Channel Modelling with MATLAB®*. London: CRC.
- Goldsmith, A. (2005). *Wireless Communications*. Cambridge University Press.
- He, C., Wang T. Q., & Armstrong, J. (2015). MIMO Optical Wireless Receiver Using Photodetectors with Different Fields of View. *Proceedings of 2015 IEEE 81st Vehicular Technology Conference*, UK.
- He, C., Wang T. Q. and Armstrong, J. (2016). Performance comparison between spatial multiplexing and spatial modulation in indoor MIMO visible light communication systems. *Proceedings of 2016 IEEE International Conference on Communications*, Malaysia.
- Hong et al. (2013). Performance of a Precoding MIMO System for Decentralized Multiuser Indoor Visible Light Communications. *Journal of IEEE Photonics*, 5(4), 7800211-7800211.
- Hong, Y., & Chen, J., & Yu, C. (2014). Performance improvement of the pre-coded multi-user MIMO indoor visible light communication system. *Proceedings of the 9th International Symposium on Communication Systems, Networks & Digital Sign*, UK.
- Hong, Y., Wu, T., & Chen, L. K. (2016). On the Performance of Adaptive MIMO-OFDM Indoor Visible Light Communications. *IEEE Photonics Technology Letters*, 28(8), 907-910.
- IEEE. (2011). *IEEE Standard for Local and Metropolitan Area Networks – Part 15.7: Short Range Wireless Optical Communication Using Visible Light*, IEEE Standard 802.15.7-2011. Retrieved from <https://standards.ieee.org>.



- IEEE. (2018). *IEEE Standard for Local and metropolitan area networks--Part 15.7: Short-Range Optical Wireless Communications – Redline*. IEEE Standard 802.15.7-2018. Retrieved from <https://standards.ieee.org>.
- Iwaizumi, H., Yoshizawa, S., & Miyanaga, Y. (2012). A new high-speed and low-power LSI design of SVD-MIMO-OFDM systems. *Proceedings of International Symposium on Communications and Information Technologies*, Australia.
- Iwaizumi, H., Yoshizawa, S. and Miyanaga, Y. (2013). A High-Speed and Low-Energy-Consumption Processor for SVD-MIMO-OFDM Systems. *VLSI Design*.
- JEITA. (2007). *CP-1221 Visible Light Communication System*. Retrieved from <http://www.jeita.or.jp>.
- JEITA. (2007). *CP-1222 Visible Light ID System*. Retrieved from <http://www.jeita.or.jp>.
- JEITA (2013). *CP-12213 Visible Beacon System*. Retrieved from <http://www.jeita.or.jp>
- Kahn, J.M., & Barry, J.R. (1997). Wireless infrared communications. *Proceedings of the IEEE*, 85(2), 265-298.
- Khan et al. (2014). A simple block diagonal precoding for multi-user MIMO broadcast channels. *Journal on Wireless Communications and Networking*, 95.
- Komine, T., & Nakagawa, M. (2004). Fundamental analysis for visible-light communication system using LED lights. *IEEE Transactions on Consumer Electronics*, 50(1), 100-106.
- Maha, B. Z., & Kosai, R. (2013). *Multi User MIMO Communication: Basic Aspects, Benefits and Challenges*. In Zid, M. B. (Ed.), *Recent Trends in Multi-user MIMO Communications* (pp.1-24). London.

- Matheus et al. (2019). Visible Light Communication: Concepts, Applications and Challenges. *IEEE Communications Surveys & Tutorials*, 21(4) 3204-3237.
- Mesleh, R., Elgala, H., & Haas, H. (2011). On the Performance of Different OFDM Based Optical Wireless Communication Systems. *Journal of Optical Communications and Networking*, 3(8), 620-628.
- Park, K. H., Ko, Y. C., & Alouini, M. S. (2011). A novel power and offset allocation method for spatial multiplexing MIMO Systems in optical wireless channels. *Proceedings of 2011 IEEE GLOBECOM Workshops, USA*.
- Pathak, P. H., Feng, X., Hu, P., & Mohapatra, P. (2015). Visible Light Communication, Networking, and Sensing: A Survey, Potential and Challenges. *IEEE Communications Surveys & Tutorials*, 17(4), 2047-2077.
- Pham et al. (2015). Sum-rate maximization of multi-user MIMO visible light communications. *Proceedings of IEEE International Conference on Communication Workshop, UK*.
- Proakis, J.G., & Salehi, M. (2008). *Digital Communications*. New York: McGraw-Hill.
- Tanaka, Y., Komine, T., Haruyama, S., & Nakagawa, M. (2003). Indoor visible light data communication system utilizing white LED lights. *IEICE Transactions on Communication.*, E86-B(8), 2440-2454.
- Xia Li, Vucic, J., Jungnickel, V., & Armstrong, J. (2012). On the Capacity of Intensity-Modulated Direct-Detection Systems and the Information Rate of ACO-OFDM for Indoor Optical Wireless Applications. *IEEE Transactions on Communications*, 60(3), 799-809.
- Wang, Q., Wang, Z., & Dai, L. (2015). Multiuser MIMO-OFDM for Visible Light Communications. *IEEE Photonics Journal*, 7(6), 1-11.

- Wang, T. Q., Sekercioglu, Y. A., & Armstrong, J. (2013). Analysis of an Optical Wireless Receiver Using a Hemispherical Lens With Application in MIMO Visible Light Communications. *Journal of Lightwave Technology*, 31(11), 1744-1754.
- Wang, T. Q., & Armstrong, J. (2014). Performance of indoor MIMO optical wireless system using linear receiver with prism array. *Proceedings of 2014 Australian Communications Theory Workshop*, Australia.
- Wang, T. Q., He, C., & Armstrong, J. (2015). Angular diversity for indoor MIMO optical wireless communications. *Proceedings of 2015 IEEE International Conference on Communications*, UK.
- Wang, T. Q., Green, R. J., & Armstrong, J. (2015). MIMO Optical Wireless Communications Using ACO-OFDM and a Prism-Array Receiver. *IEEE Journal on Selected Areas in Communications*, 33(9), 1959-1971.
- Wang et al. (2015). Multi-user MIMO-OFDM for indoor visible light communication systems. *Proceedings of IEEE Global Conference on Signal and Information Processing*, USA.
- Wang, Q., & Wang, Z., & Dai, L. (2015). Multiuser MIMO-OFDM for Visible Light Communications. *Journal of IEEE Photonics*. 7(6), 1-11.
- Wang, T. Q., He, C., & Armstrong, J. (2017). Performance Analysis of Aperture-Based Receivers for MIMO IM/DD Visible Light Communications. *Journal of Lightwave Technology*, 35(9), 1513-1523.
- Wilkins, A, Veitch, J., & Lehman, B. (2010). LED lighting flicker and potential health concerns: IEEE standard PAR1789 update, *Proceedings of 2010 IEEE Energy Conversion Congress and Exposition*, USA.

## BIODATA



- Name-Last name:** Jariya Panta
- Address:** Faculty of Industrial Technology,  
Ubun Ratchathani Rajabhat University,  
Nai Mueang, Muang Ubun Ratchathani,  
Ubun Ratchathani, 34000.
- Email:** jariya.panta@gmail.com
- Contact number:** +66851231508
- Education Background:**
- Masters of engineering degree (M.Eng.) in Telecommunications from the school of engineering and technology, Asian Institute of Technology (AIT), Pathumthani, Thailand, in 2014.
  - Bachelor of engineering degree (B.Eng.) from the Department of Electrical and Electronic Engineering, Faculty of Engineering, Ubun Ratchathani University (UBU), Ubun Ratchathani , Thailand, in 2011.

**Bangkok University**

**License Agreement of Dissertation/Thesis/ Report of Senior Project**

Day 11 Month August Year 2022

Mr./ Mrs./ Ms. Jariya Panta now living at 103  
Soi - Street Warin-Det  
Sub-district That District Warinchamrab  
Province Ubonratchathani Postal Code 34190  
being a Bangkok University student, student ID 9590900024  
Degree level  Bachelor  Master  Doctorate  
Program Electrical and Computer Engineering Department Engineering  
School Graduate School hereafter referred to as “the licensor”

Bangkok University 119 Rama 4 Road, Klong-Toey, Bangkok 10110  
hereafter referred to as “the licensee”

Both parties have agreed on the following terms and conditions:

1. The licensor certifies that he/she is the author and possesses the exclusive rights of dissertation/thesis/report of senior project entitled Performance Optimisation and Efficient User Grouping of MU-MIMO for Indoor Optical Wireless Communication Systems submitted in partial fulfillment of the requirement for the Degree Doctor of Engineering in Electrical and Computer Engineering of Bangkok University (hereafter referred to as “dissertation/thesis/ report of senior project”).
2. The licensor grants to the licensee an indefinite and royalty free license of his/her dissertation/thesis/report of senior project to reproduce, adapt, distribute, rent out the original or copy of the manuscript.
3. In case of any dispute in the copyright of the dissertation/thesis/report of senior project between the licensor and others, or between the licensee and others, or any other inconveniences in regard to the copyright that prevent the licensee from reproducing, adapting or distributing the manuscript, the licensor agrees to indemnify the licensee against any damage incurred.

This agreement is prepared in duplicate identical wording for two copies. Both parties have read and fully understand its contents and agree to comply with the above terms and conditions. Each party shall retain one signed copy of the agreement.

Jariya Panta Licensor  
( Jariya Panta )

อภัยม Licensee  
(Director, Library and Learning Center)

[Signature] Witness  
(Dean, School of Engineering)

[Signature] Witness  
(Program Director)

